Master's thesis

NTNU
Norwegian University of Science and Technology
Faculty of Engineering
Department of Mechanical and Industrial Engineering

Simon Folkman Hedland

Electrochemical Impedance Spectroscopy for Organic Coating Assessment

Master's thesis in Subsea Technology
Supervisor: Ole Øystein Knudsen
Co-supervisor: Andreas Løken, Anders Skilbred
December 2021

NTNU
Norwegian University of Science and Technology

Simon Folkman Hedland

Electrochemical Impedance Spectroscopy for Organic Coating Assessment

Master's thesis in Subsea Technology
Supervisor: Ole Øystein Knudsen
Co-supervisor: Andreas Løken, Anders Skilbred
December 2021

Norwegian University of Science and Technology
Faculty of Engineering
Department of Mechanical and Industrial Engineering

NTNU
Norwegian University of
Science and Technology

Preface

The master's thesis *Electrochemical Impedance Spectroscopy for Organic Coating Assessment* was carried out at the Department of Mechanical and Industrial Engineering in the Norwegian University of Science and Technology (NTNU). It is a finalization of a master's degree programme in Subsea Technology, with specialization in Subsea Operation and Maintenance. The work was carried out in collaboration with Jotun. It was supervised by Professor Ole Øystein Knudsen (Department of Mechanical and Industrial Engineering), Andreas Løken (Jotun) and Anders Skilbred (Jotun). The experimental work was conducted at the Department of Materials Science and Engineering at NTNU.

Acknowledgements

I would like to thank my supervisor, Professor Ole Øystein Knudsen, for bringing his invaluable experience and knowledge to this project. He never failed to give advice and support.

I gratefully acknowledge Jotun for the opportunity to collaborate on this work. I would like to thank my supervisors at Jotun, Andreas Løken and Anders Skilbred, for their guidance and many enjoyable meetings.

Finally, I would like to thank Andreas Erbe, Anita Storsve, Bo Qin and Johannes Ofstad, who provided first-class facilities and help at the Department of Materials Science and Engineering laboratories.

Abstract

Electrochemical Impedance Spectroscopy (EIS) is an electrochemical technique that has been used for decades in research. There are signs that the coatings industry is gaining interest in EIS, and the technique is becoming more widely utilized. The main objective of this thesis was to assess organic coating barrier properties and performance with the use of EIS. Further, a procedure for routinely usage of EIS as part of a test regime on organic coatings was developed. Previously published work was reviewed to determine the correlation between impedance and coating parameters that influence cathodic disbondment (CD). Also, external factors that influence CD on organic coatings like temperature, applied potential and electrolyte exposure was investigated.

Six organic coatings were exposed to an electrolyte and subjected to heating and thermal cycling with applied cathodic potential. EIS was used to measure the impedance of the coatings during the experiments. It was observed that the impedance of all coatings decreased as an effect of increase in temperature. Coatings with higher film thickness displayed less decrease in impedance as an effect of increase in temperature. The impedance of a coating with higher glass transition temperature (T_g)-region was less affected by increase in temperature and total reversible impedance was observed in thermal cycling. A correlation between high impedance and resistance to CD was established.

Sammendrag

Elektrokjemisk impedans spektroskopi (EIS) er en elektrokjemisk metode som har blitt brukt i flere tiår i forskning på maling. Malingsindustrien viser økt interesse for metoden, og den blir stadig tatt mer i bruk. Hensikten med denne oppgaven var å undersøke barriereegenskapene til maling med EIS. Det ble etablert et oppsett og en metode for å bruke EIS som en rutinemessig del av et testregime for maling. Det ble foretatt en studie av publisert arbeid for å fastslå sammenhengen mellom impedans og parametere på maling som påvirker katodisk avbinding. Ytre faktorer som påvirker katodisk avbinding ble også undersøkt, slik som temperatur, påført potensial og eksponering for elektrolytt.

Det ble utført eksperimenter på seks ulike malingssystemer. Malingsprøvene ble eksponert for en elektrolytt med påfølgende oppvarming og termisk sykling med påført katodisk potensial. EIS ble brukt til å måle impedans på malingene under eksperimentene. Det ble observert at impedans sank på alle malingene som en effekt av økt temperatur. Impedans på maling med høyere filmtykkelse var mindre påvirket av økt temperatur enn tilsvarende maling med lavere filmtykkelse. Impedans på en maling med høyere glass-transisjonstemperatur var mindre påvirket av økt temperatur, og viste reversibel impedans under termisk sykling. Det ble fastslått en sammenheng mellom høy impedans og motstand mot katodisk avbinding.

Contents

1 Introduction

1.1 Background

Measurement techniques based on electrochemistry, such as electrochemical impedance spectroscopy (EIS) have for several decades been used to assess different coating properties. Although the various techniques are very promising and powerful in terms of providing high quality quantitative data, they are also renowned for being inaccessible and difficult to interpret. However, there are clear signs showing that the industry is gaining interest in such techniques as EIS.

1.2 Problem Description

The majority of data and results of coating assessment with EIS presented in test reports and literature today yields little insight to coating degradation. This is mainly due to the lack of industry standards, lack of knowledge on how to interpret and analyze the results, and lack of knowledge and experience regarding the possibilities and limitations of EIS. Jotun is a coating manufacturer that sees electrochemical techniques as a possibility to meet the industry's need for assessing coating performance. More specifically, there is a demand for establishing a robust and reliable procedure for measuring coating performance with EIS.

1.3 Objectives and Scope

The primary objective of this thesis was to explore how the barrier property of coatings are affected by temperature using EIS measurements. This was to ultimately gain a better understanding of coating performance as a function of temperature. Other parameters such as film thickness, number of coats, aluminium pigments, and glass transition temperature were also investigated. Based on this work, a proposed procedure based on EIS was to be developed for routinely characterizing coatings as part of Jotun's test regime to determine inherent barrier properties of organic coating. The objective was tackled by both reviewing existing literature on the use of EIS in coating assessment, and by conducting experimental work on coating samples provided by Jotun. The results were interpreted to determine the

effect of temperature and thermal cycling on impedance, as well as the correlation between impedance and cathodic disbondment (CD).

2 Theory

2.1 Cathodic Disbonding

Cathodic disbonding (CD) is a mechanism that causes a coating to lose adhesion, thereby reducing its protective property. Even though CD has been thoroughly studied [1, 2], there are still details on what happens at the interface between the coating and the metal that are not yet fully understood. The electrolytic resistance of a coating prevents elechtrochemical cathodic reactions from occuring on the metal substrate. Impedance measured on a coating indicate its electrolytic resistance. CD is often initiated on areas where the coating film is degraded or areas that have mechanical damages, as well as sharp edges where the coating film is thin [3, 4].

CD is a degrading process that reduces the adhesion of an organic coating to the substrate it is applied on, either by a mechanical damage or a weakness in the film. When the electrolytic resistance of a coating is lowered or the film is damaged, ions can migrate though the film and cathodic oxygen reduction can take place on the coating/oxide layer interface. This causes disbonding of the coating. The chemical reaction that takes place can be expressed with this equation:

$$O_2 + 2H_2O + 4e^- = 4OH^- \tag{2.1}$$

The hydroxide ($4OH^-$) causes the binding between coating and substrate to break, and the coating looses adhesion to the substrate. Due to hydroxide accumulating between the coating and the substrate, an electrolyte with high pH can be observed in this area. There is a consensus among researchers of CD that this local alkalinity is causing coating disbondment [5]. It has earlier been proposed that dissolution of oxide layer could be causing CD. However, CD also occurs on metals that have stable oxide layer. Another theory suggests that free radicals and peroxides that are formed intermediately in the cathodic reaction causes disbondment. Free radical scavengers and peroxide decomposers have been added to generic types of coating to prevent CD with limited success [6]. It is hard to prove that these

intermediate products are causing the disbonding as they also tend to prevent hydroxide formation [4].

Coated steel structures that are submerged, may be polarized down to -1150 mV vs $Ag/AgCl$ potential with cathodic protection. The cathodic reaction that occurs under the coating could potentially be both hydrogen evolution and oxygen reduction. However, the dominating cathodic reaction under organic coatings is the oxygen reduction reaction for such potentials. Previous work has proven that significant hydrogen evolution under organic coatings tend to be present when the potential is lower, i.e. more negative than -1150 mV [4].

The cathodic reaction described in equation (2.1) can occur as ions are transported through the coating and thereafter in the aqueous film under the disbonded coating to the disbonding front. There is a consensus that ions are not transported through organic coatings unless the electrolytic resistance of the coating is low. A coating with over 10^9 Ω resistance is considered impermeable to ions [7]. At lower resistance, typically under 10^6 Ω, organic coatings are to a degree permeable to ions [8-10]. Cations are transported to the site of the cathodic reaction to neutralize the negative charge produced by the reaction. In seawater, sodium (Na^+) balance the cathodic reaction and sodium hydroxide is produced [4].

Transport of cations to the disbonding front has been discussed in various studies that have concluded differently. This issue is important because CD could in theory occur under the undamaged coating if both cations and anions are transported through the coating to the metal substrate. Studies where coatings have been tested under free corrosion have concluded that cations were transported in an aqeous film under the disbonded coating [11]. Cathodically polarized coated steel with film thickness as low as 10 µm has been tested by Leidheiser [12]. Based on quantitative results, it was concluded that cation transport through the coating occurs during cathodic polarization of coated samples, and that this is the rate controlling step in CD. The effect of cathodic polarization on ionic migration through organic coatings has been studied by Leidheiser and Parks [13]. Samples were cathodically polarized at -800 mV vs $Ag/AgCl$ and were observed to take up 3-28 times the of ions compared to the same tests performed under open circuit potential. Their conclusion then was that ionic migration through the coating was sufficient itself to explain the CD rate observed from the test results. The prevailing argument is currently that most cations are not transported through organic coating [4]. Cations have been demonstrated to migrate under the disbonded coating and thereafter transported to the disbonding front, as illustrated in Figure 1 [5, 6].

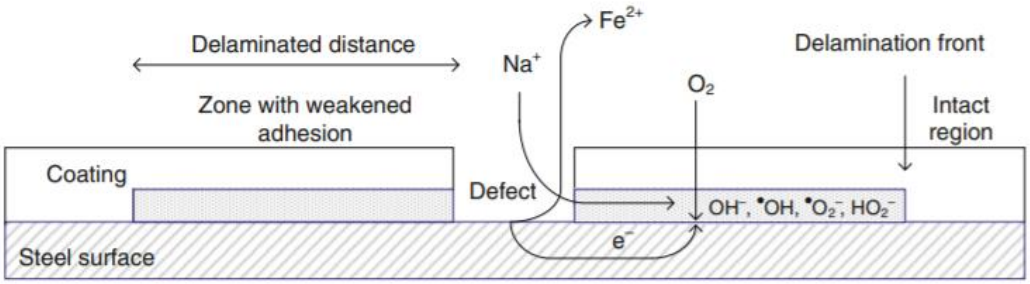

Figure 1: A simplified figure that demonstrates CD [6].

The CD process starts in areas where the steel is exposed to an electrolyte. This can be on holidays in the coating caused by mechanical damage, blisters, edges and other areas where bare metal is exposed to the electrolyte. For structures that have cathodic protection, electrons are transported from the sacrificial anode to the steel and the anodic reaction occurs on the sacrificial anode. CD also occurs on structures that do not have cathodic protection. In such cases, the anodic reaction is the dissolution of the metal that is likely to occur in the location where the coating is damaged. It can be hard to detect CD without peeling off the disbonded coating because the gap between substrate and coating may only be a few micrometers wide [4].

2.1.1 Resistance of Organic Coatings and Factors of CD

The aim of this section is to present some of the research conducted on a selected number of parameters related to CD. Not all known factors could be discussed, as it would be beyond the scope of this thesis. Existing findings are presented topic by topic. The subject of resistance of coatings is devoted much attention, as it is of special importance to this thesis.

There is a general consensus that a good working coating with sufficient barrier property should typically have over $10^9\ \Omega \cdot cm^2$ resistance [12, 14]. According to the work of Bacon et al. [15] and Bierwagen et al. [7], coatings with less than $10^6\ \Omega \cdot cm^2$ displayed poor barrier property and low protection of substrates. Organic coatings that are in use will often be subjected to variations in temperature and electrolyte solution concentration in real-world settings. Such cyclic environmental factors causes both pysical and chemical degradations to the coatings [16].

As previously elaborated, CD is a mechanism that requires cation as well as anion transport. The reaction that causes the disbonding takes place as cations are transported beyond the disbonding front. The electrochemical potential distribution as a function of time and distance from a coating defect is shown in Figure 2. Three characteristic areas with respect to potential can observed in the diagram. The high potential on the right-hand side is associated with the adhering coating. Moving to the left, a sudden drop in potential is apparent. This is the potential correlating with the disbonding front of the coating. To the left-hand side of the sudden drop in potential, a lesser decrease in potential is seen due to the resistance of the electrolyte under the disbonded coating. The potential gradient in the disbonding front drives cations under the adhering coating and is possibly the mechanism that drives CD [4]. Knudsen et. al. [17] has introduced a hypotheses that the bulk coating resistance measured as impedance correlates to the resistance against migrating cations under the adhering coating and limits CD.

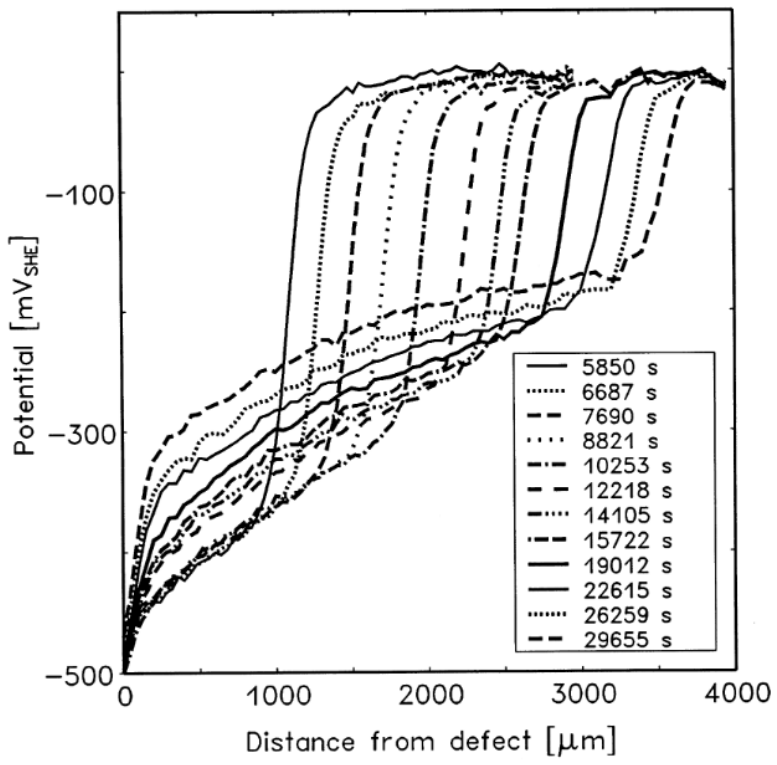

Figure 2: Potential distribution under a coating as a function of time and distance from the original coating defect during a CD experiment, measured with scanning kelvin probe(SKP) [18].

A strong correlation between coatings performance on CD tests and measured impedance was indicated in the same study by Knudsen et. al. [17]. Coating samples were CD-tested and EIS

was performed in accordance with ISO 15711 and ISO 16773-2 respectively. The results plotted in Figure 3 suggests that a coating system with high measured impedance will have a low rate of disbonding in a CD test.

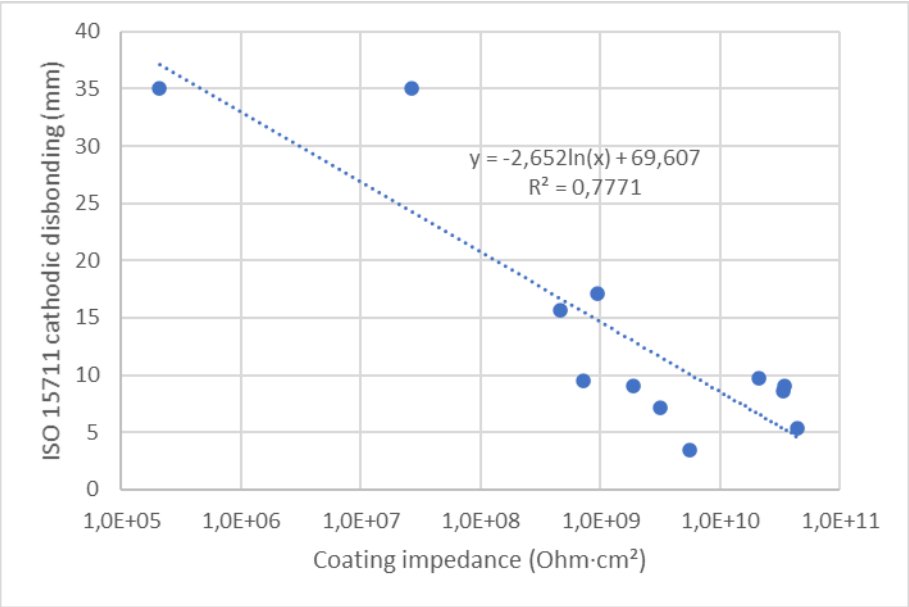

Figure 3: Research results showing a correlation between CD and impedance[17].

The Effect of T_g

Temperature is one of the factors that has been studied and proven to affect coating resistance to CD. Temperatures above Tg will cause decrease in the electrolytic resistance of an organic coating and increased rate of CD [3]. In this thesis, Tg is often referred to as a specific temperature where the polymer network of a coating begins to shift from a glassy to a rubbery state upon heating, and vice versa upon cooling. It should be noted, however, that polymers have a temperature range where this transition takes place gradually. This is referred to as the Tg-region [19].

A study by Shreepathi [20] investigated how CD resistance of coatings is related to applied cathodic potential, film thickness and temperature. Pigmented high-build epoxy coating was applied on steel panels with dry film thickness (DFT) ranging from 150μm to 500 μm in CD-testing. Measurement of the coating T_g was also done by differential scanning calometry (DSC) and was determined to be $\sim$ 55℃. The testing was conducted in accordance with ASTM G8, G42 and G95. However, Shreepati added that some of the ASTM methods were conducted with a modification of higher temperature and applied cathodic potential. Coated

panels were attached to an electrochemical cell containing either a mixture referred to as 'triple salt' (1 wt % each of $NaCl, Na_2CO_3$ and Na_2SO_4) or simply 3 wt % $NaCl$. The cell with coatings attached was heated in an oven to either 60 or 90℃ and a cathodic potential of -1500 mV vs SCE was applied. Duration of the exposure to heated electrolyte was between 3 and 30 days, after which the samples were evaluated with respect to CD. An excerpt of the results from experiments carried out in the study is listed in Table 1, representing the general conclusion in the study that temperatures above Tg result in increased CD, and that coating thickness is significant to CD as well. This is observed even over short periods of testing, such as three days.

Table 1: CD-testing parameters and Results [18].

DFT (µm)	Temperature (℃)	$E_{SCE}(mV)$	Method (ASTM)	Duration (Days)	Disbonding radius (mm)
150	RT	-1500	G8	30	36
200	RT	-1500	G8	30	31
400	RT	-1500	G8	30	2
200	60	-1500	G42	10	30
400	60	-1500	G42	30	42
400	RT	-1500	G95	30	35
400	90	-1500	G95(modified)	3	40

The effect of temperatures above T_g on coatings according to Shreepati, is that coating properties change significantly. The extensive work of Leidheiser [12] suggests that the pore diameter in organic coating films increase as the coating is exposed to an electrolyte over time and water penetrates more extensively into the coating. When the pore diameter increases, the measured resistance of the coating decrease. In other words, exceeding T_g softens the coating and it becomes more water permeable. This increases the cathodic reaction sites on the interface between coating and metal. Hydrogen generation may take place at these sites and a pressure can develop in the interface between coating and metal, which forces coating upwards and results in visible blisters. Blisters can also protrude because of ion formation that causes a concentration gradient between the interface and bulk electrolyte that makes an osmotic pressure. Formation of such blisters means that CD testing must be terminated. The study concluded that when coatings are subjected to temperatures above T_g they more likely to display increased rates of CD.

The immersion of coatings in water can have a decreasing effect on T_g, as proven by Mijovic and Lin[21]. Decrease of T_g while a coating is immersed is dependent on water uptake. According to Birwagen et. al. [7], T_g decrease is related to features of coatings such as porosity and hydrophilicity. Decrease of coating T_g will get larger with increased water content in the coating to the point where the coating is saturated with water.

Thermal Cycling

As coatings are subjected to heat and water over time, hygrothermal aging occurs. This is a degradation mechanism where coatings swell permanently. Epoxy coatings are especially prone to temperature induced degradation. However, During thermal cycling over short periods where coatings are immersed, they are likely to show signs of recoverable aging effects such as softening and plasticization [22, 23].

Bierwagen investigated the effect of thermal cycling on organic coatings [7], specifically changes in T_g. A testing cycle was developed (Figure 4) and repeated three times with coating samples while they were immersed. After three runs of thermal cycling, the coatings were immersed in room temperature for three days. The total testing was conducted within a week.

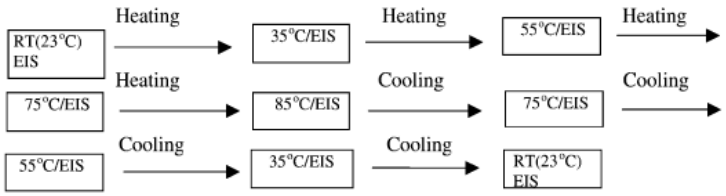

Figure 4: Schematic of one thermal cycle proposed by Birwagen[7]. The total thermal cycling test consisted of three thermal cycles.

Epoxy coating samples showed a decrease in T_g of about $15 - 20℃$ as an effect of thermal cycling, while a chromated coating showed a decrease of about $20 - 30℃$. The impedance of the samples decreased as an effect of increased temperature but reversed when cooled down to room temperature. The study concluded that reversible impedance during thermal cycling indicated that the corrosion resistance of the samples was good. Reversibility of impedance during thermal cycling is an indication of water uptake resistance in coating systems and

adhesion retainment between the coating and substrate. Irreversible decrease of impedance in thermal cycling indicates degraded barrier properties of organic coatings.

Film Thickness and Aluminium Pigmentation

A factor that is evidently important regarding the risk and rate of CD is coating film thickness. NORSOK standard M-501 6th edition specifies a minimum criterion for coatings applied on offshore installations on the Norwegian continental shelf. For submerged carbon- and stainless steel (7B), a minimum of two coats with a total DFT of 350μm is required. This is commonly regarded as a measure that reduces risk of CD but cannot completely prevent it [4].

There is a proven correlation between the film thickness and the resistance of coatings, measured as impedance with EIS. Shreepati has found that the measured coating resistance will increase linearly with film thickness [20]. Bierwagen [16] has proven that an increase in thickness of thin films will result in a small increase in resistance up to a certain critical thickness where resistance increases drastically. Above the first critical thickness, a slow increase in resistance is seen again until a second critical thickness where resistance increase rapidly along with the thickness [9, 16]. Gonzáles et al. [24] demonstrated a similar second critical film thickness in a study where an epoxy primer of three different thicknesses were measured by EIS after being exposed to 3 wt % $NaCl$ for long periods of 1500 hours. A low resistance of $10^4\ \Omega \cdot cm^2$ was measured on a thin coating of 100 µm after exposure to the electrolyte. The two other coatings on the other hand, with thickness 200 μm and 500 μm respectively, were able to retain almost the same resistance of over $10^8\ \Omega \cdot cm^2$ after exposure to the electrolyte. The findings of Shreepati [20] were also that the resistance of some coatings is linearly dependent of thickness up to a certain threshold thickness, where increased thickness cannot provide more protection against CD.

Knudsen and Steinsmo [25] investigated mechanisms of aluminium pigments in coating on steel to explain the effects related to reduced CD. By increasing alumnium pigments in coating up to 10%, a six-fold decrease in the oxygen diffusion rate was observed. The oxygen permeability of the coating was little affected. A small decrease in water diffusion rate was shown. The ionic conductivity of the coating was increased by increasing the aluminium pigmentation concentration. The effect of reduced CD by adding aluminium pigments in the

coating could only be observed for the first layer of coating. Knudsen and Steinsmo interpret this as an indication that aluminium pigments are chemically active in decreasing CD and therefore need to be present at the interface between coating and substrate. This means that aluminium pigments do not affect the barrier properties of coatings.

Cathodic Potential

By subjecting a coating of two different thicknesses (20 µm and 120 µm) to different potentials, Jin et al. [26] investigated how the CD rate was affected by changes in the potential. Potentials between -600 and -1350 mV vs SCE were applied. Both films exhibited a CD rate, which linearly increased upon lowering the potential. In the experiments by Shreepati previously referred to [20], the effect of cathodic polarization on CD was investigated. Samples were polarized to potentials ranging from -1000 to -2500 mV vs $Ag/AgCl$, while keeping other parameters constant. An increase in cathodic potential resulted in higher rates of CD, regardless of DFT. Even samples with film thickness of 400 μm displayed a fast increase in disbonding radius as the applied potential was lowered from -1500 to -2500 mV vs $Ag/AgCl$. Contrary to Knudsen and Skar [5], Shreepati did not observe that the disbonding rate was linearly dependent with applied potential. The potential range applied by Shreepati was lower than that of Knudsen and Skar (-750 and -1400 mV vs SCE). Moreover, some of the samples tested were also tested at different electrolyte temperatures, being 60 ℃ in Shreepati's work, while Knudsen and Skar tested at 25 ℃. These factors offer an explanation to the difference in results. The effect of testing at higher temperatures along with applied cathodic potential is seen in Figure 5.

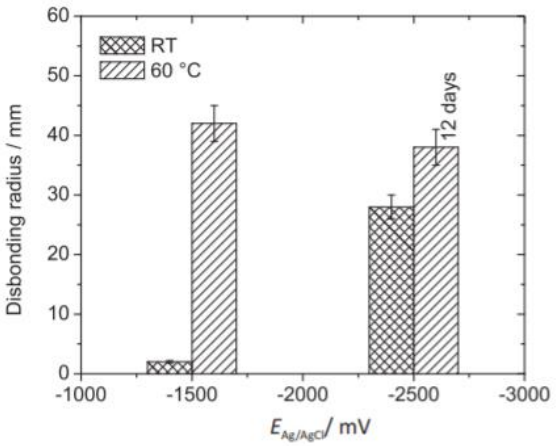

Figure 5: The effect of cathodic potential and temperature on coating with 400 µm DFT in triple salt solution. Tests performed with -1500 mV and -2500 mV at RT lasted for 30 days [20].

It should be further noted that the CD testing carried out by Shreepati at low potential and high temperature suffered from blistering and cracking of coating and was therefore terminated within 12 days.

When cathodic potential is applied, the disbondment front will have a higher potential than the applied potential (see Figure 2). The potential on the exposed metal in the original damage and the applied potential will be close to equal [11]. As explained previously, this is due to resistance in the electrolyte. The potential in the disbondment front will, however, be affected by the applied potential [5].

Electrolyte

The chemical composition of the electrolyte is an important factor that can have great effect on CD. If oxygen is not present in the electrolyte, oxygen reduction under the coating will not occur and disbonding of coating does not take place. This subject was investigated by Stratman et al. [11] by examining an unpigmented alkyd resin with SKP in an argon-atmosphere. It has been proven that if oxygen is not present in an electrolyte where coated steel is placed, CD is not initiated under free corrosion potential. CD was initiated after argon was replaced with oxygen. Leidheiser and Wang [3] observed very low rates of CD during an experiment where samples were polarized to -1350 mV vs SCE and oxygen concentration was very low in the electrolyte. This was obtained by purging the electrolyte of oxygen by bubbling nitrogen through the electrolyte. Knudsen and Skar [5] tested the effect of oxygen

concentration on two epoxy coatings with DFT of 171 +/- 13 µm and 167 +/- 13 µm. Samples were polarized to -1050 mV vs SCE while exposed to substitute seawater saturated with pure oxygen or air. The coated samples exposed to the electrolyte saturated with pure oxygen showed significantly larger aeras of disbondment due to CD.

Cations must be present at the site of the oxygen reduction reaction to maintain charge balance. The type and concentration of cations in the electrolyte influences the rate of disbonding. Leidheiser et al. [27] studied the migration of cations to the reaction site. An epoxy coating was permitted to disbond off a steel surface from a defect under a free corrosion potential. After the coating had delaminated, it was removed and the aqueous phase on the substrate surface was dried. By using Auger spectroscopy, the amount of species located at a remote point from the defect was identified. The findings showed that the disbonding rate of the coating was linearly related to the diffusion coefficient of cation type in aqueous solution. Knudsen and Skar [5] demonstrated that the disbonded area on an epoxy coating is linearly dependent on molar conductivity of the cation in electrolyte solution. The higher mobility the cation has in water, the greater will the disbondment rate be. It was pointed out by Knudsen and Skar that various studies often interpret this as proof that the transport of cations is a rate limiting factor of CD [13].

2.2 Electrochemical Impedance Spectroscopy

Resistance has been used to evaluate coating properties since the late 1930s. DC-resistance was used to determine the performance of coatings and simple classification like ‘good’, ‘fair’ and ‘poor’ was eventually handed to different coating systems in the late 1940s. The assumption that the protection of coatings submerged in seawater was related to electrolytic resistance was established. Mengers and Schneider were some of the first to apply EIS as a technique to research coating properties, and the technique has since been used frequently in published studies [9].

Several factors have caused the use of EIS to develop further in recent years. Importantly, the accuracy of the instrumentation has increased significantly and measuring and recording of data is now automated. Software for analyzing measured data has also improved in recent years. The combination of these factors has made EIS a powerful tool in coating research [15].

2.2.1 EIS for Evaluating Coating Performance

EIS is one of the most frequently used electrochemical techniques to determine the protective properties of organic coatings. The technique works by perturbing an AC signal on a test specimen to observe its equivalent impedance. The electric response to the AC signal of the specimen is monitored, as various frequencies are applied. Impedance will typically be measured at frequencies ranging from 100 mHz down to 10 mHz [9, 28].

A great advantage EIS has compared to other electrochemical techniques, is that it can be conducted over a short time because it is very sensitive, in addition to indicating details on the mechanisms of corrosion. There is currently a need to predict the performance of coatings before the actual degradation has taken place. EIS is a technique that indicates the electrolytical resistance of a coating, which is useful to evaluate degradation [9].

2.2.2 EIS Principle

The word impedance describes a system's opposition to a perturbation from its steady state. The perturbation is in the form of an alternating voltage and the impedance is the current response measured. A DC bias potential is the applied signal which a sinusoidal perturbation E_t (2.2) is superimposed onto. It can be said that impedance is resistance depending on frequency, or the equivalent of DC resistance for an AC system [9].

$$E_t = E_0 \sin \omega t \text{ [9]} \qquad (2.2)$$

Angular frequency ω:

$$\omega = 2\,\pi f \text{ [9]} \qquad (2.3)$$

The current response will be sinusoidal for a linear time-invariant system and has a phase shift ϕ:

$$I_t = I_0 \sin(\omega t + \phi) \text{ [9]} \qquad (2.4)$$

Impedance Z dependent on angular frequency ω, is the ratio of sinusoidal perturbation over current response:

$$Z(\omega) = \frac{E_t}{I_t} \text{ [9]} \qquad (2.5)$$

Complex numbers can be used to explained impedance. This is because both magnitude and phase of the current affect impedance. The complex notation j is equal to $\sqrt{-1}$, and a common expression for impedance is therefore also:

$$Z(\omega) = \frac{E_0 \exp(j\omega t)}{I_0 \exp(j\omega t + \phi)} = |Z| \exp(j\phi) \text{ [9]} \quad (2.6)$$

Impedance Z at frequency ω can be defined as a vector in the complex plane of magnitude $|Z|$. There is an angle ϕ between the vector $|Z|$ and the real impedance resistance Z' axis in this plane. An imaginary part, reactance, is represented by Z''. Reactance is an oppositional property in AC that creates a 90° phase shift between voltage and current [29]. Therefore, impedance can be expressed as follows:

$$Z(\omega) = Z' + jZ'' \text{ [9]} \quad (2.7)$$

To process, display and interpret EIS data, it is important to keep in mind that impedance can be expressed with both equation (2.6) and (2.7). This is discussed in section 2.2.5

2.2.3 Electrochemical Cell Testing

An electrochemical cell can be used in EIS measurements of coatings. The cell can have different shapes but is electrochemically inert and will typically have the coated metal specimen attached to it and some type of electrolyte exposure. The coated metal is the working electrode (WE). A platinum mesh or thread can be placed parallel to the coated metal surface and acts as counter electrode (CE). A reference electrode (RE) must also be present in the cell [9].

Between the CE and the WE, a sinusoidal voltage perturbation is applied. A potentiostat is used for control during the measurements. One approach can be to keep DC potential relative to RE equal to the open circuit potential (OCP) [9]. For investigating organic coating properties and failure, coated panels have commonly been cathodically polarized. The aim can be to simulate offshore situations where structures are submerged and surfaces of organic coated steel are often cathodically polarized using sacrificial anodes or an impressed current system [8].

2.2.4 EIS Elements

The measured impedance in EIS reflects physical properties of the testing cell. These properties can be divided into elements that are possible to identify and interpret [28].

The electrolyte in the testing cell contains ions that will have a certain resistance. This resistance is called the solution resistance and will vary with factors such as ionic concentration, type of ions, temperature but also depending on the geometry of the area where current is moving [28]. The resistivity ρ resulting from different concentrations of $NaCl$ can be determined by standard chemical listings, and the solution resistance R can be calculated from equation (2.***8***, assuming that the current is uniform in a bounded volume with the cross-sectional area A and length l:

$$R = \frac{\rho l}{A} \text{ [28]} \qquad (2.8)$$

During EIS testing, ions from the electrolyte solution attach to the electrode surface. This is called an electrical double layer. There is only a small separation between these layers but due to the insulation, charges are separated. This forms a capacitor with approximately 20-40 μF capacitance per cm^2 of electrode area [30]. A few factors may affect the double layer capacitance, such as the potential of the electrode, temperature of the electrolyte in the testing cell, type of ions in the electrolyte, oxide layers, absorption of impurities and how fine the electrode surface is polished [28].

Pore resistance (R_p) is an important element in coating assessment with EIS. R_p indicates the resistance to electrolyte penetration through microscopic pores, or areas where cross-linking of the polymer is inadequate [31]. The magnitude of R_p indicates the barrier properties of the coating, and decreases with coating degradation [9].

EIS can be modeled with a Randle's cell in a simple way. This is the most common way to model EIS and can be used as basis for modeling coated metal. How to model coated metal has caused controversy for a long time. the equivalent impedance of a coated metal can be simplified and modelled [28], as shown in Figure 6.

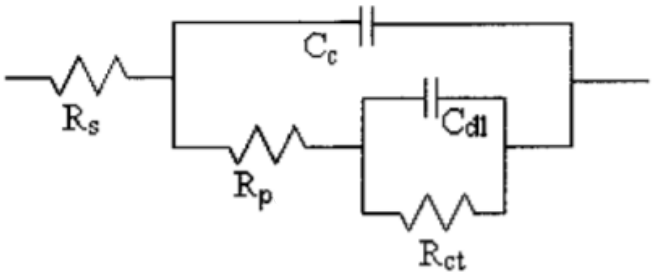

Figure 6: Coated metal electrical model [28].

This model includes solution resistance (R_s), double layer capacitor (C_{dl}) represented by a constant phase element (CPE), Charge transfer (R_{ct}), R_p and capacitance of an undamaged coating (C_c). The behavior of a coating is hard to model due to degrading over time. This becomes even more complex when water penetrates the coating and reaches the metal surface and forms a new interface [28].

2.2.5 EIS Data Representation

EIS data is regularly analyzed by using a so-called phenomenological approach. This involves interpreting EIS data by applying an electrical equivalent circuit. The circuit is made up of elements that have the purpose of retaining the electrical characteristics that are expected from measured EIS data [9].

The impedance data measured in an electrochemical cell is complex valued. It consists of a magnitude and a phase, meaning that plotting methods are a challenge for analyzing the data graphically. Impedance data collected by EIS is normally represented in either a Bode plot or a Nyquist plot [9].

For organic coatings, a Bode plot is commonly used to display the impedance spectra for analyzing properties. A Bode plot has the magnitude $|Z|$ plotted versus the applied frequency f on one pair of axes and phase ϕ versus applied frequency f on the second axes. What is popularly referred to as a 'Nyquist plot' is based on equation (2.7*)*, and represents EIS data in a complex plane [9]. The basis for such a plot is the Argand diagram, as illustrated in Figure 7.

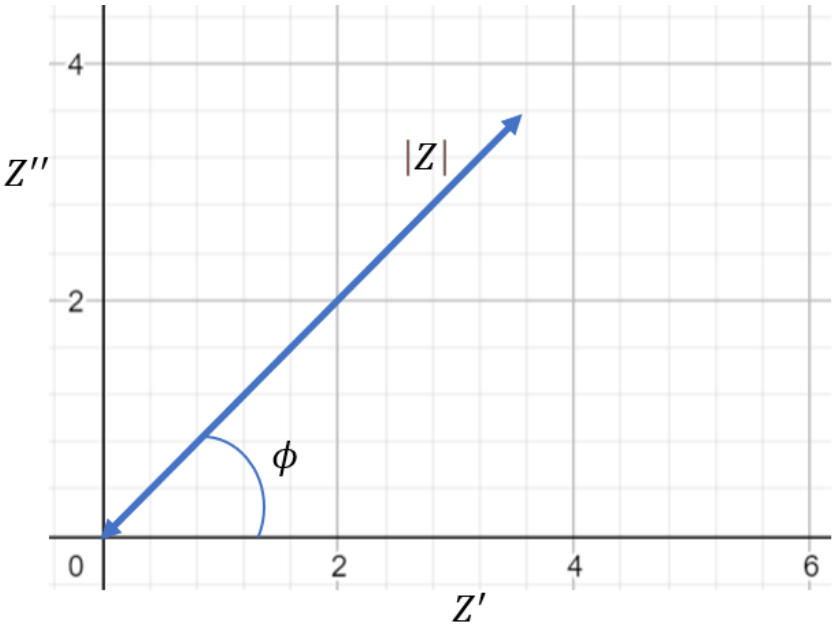

Figure 7: An Argand diagram that forms the basis for a Nyquist plot. The vector $|Z|$ is composed of a real part Z' and an imaginery part Z''.

The use of complex plane plots, such as Nyquist plot can be less advantageous and sometimes misleading when interpreting results from coating tests with EIS. Impedance data displayed in a Bode plot is shown in Figure 8, where a coating displays a decrease in impedance measured from curve (1) to curve (3). This indicates degradation of coating by decrease in R_p [32]. The face shift ϕ of each impedance measuring in Figure 8 is shown in Figure 9.

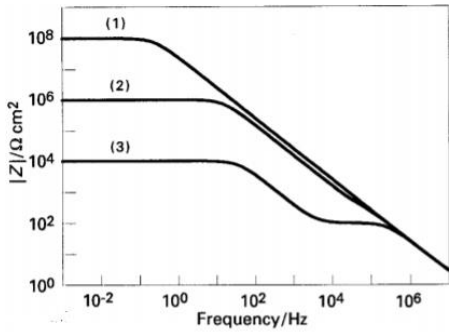

Figure 8 Theoretical Bode plot displaying magnitude versus frequency [32].

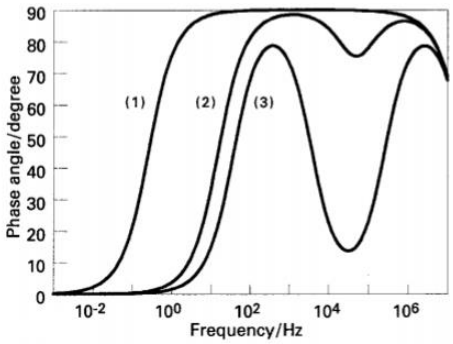

Figure 9 Theoretical Bode plot displaying change in face angle versus frequency [32].

The data from Figure 8 and Figure 9 are also displayed in a Nyquist plots in Figure 10. It can be observed that these Nyquist plots do not allow clear indication of coating degradation. However, this may be achieved by plotting high frequency data separately [32].

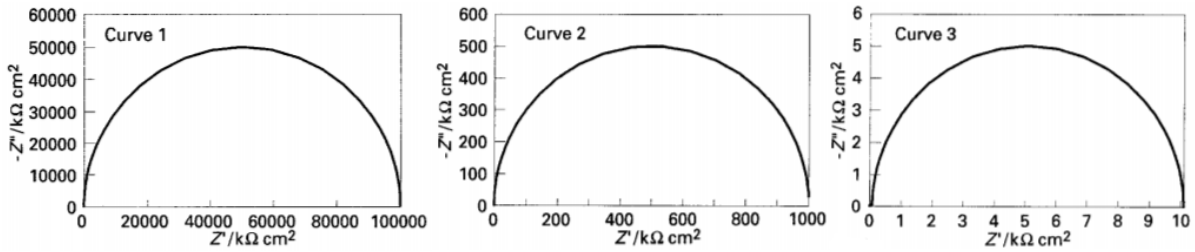

Figure 10: Nyquist plots displaying values of real part $\boldsymbol{Z'}$ (real impedance) versus imaginary part $\boldsymbol{Z''}$ (reactance)[32].

Studies that use EIS to assess coating properties [7, 12, 16, 20] commonly refer to the impedance measured at 10 mHz displayed in a Bode plot, as it typically represents R_p of the coating. A bode plot with the impedance spectrum of an organic coating is shown in Figure 11. The impedance measured at 10 mHz indicates a R_p in the range of $10^8\ \Omega \cdot cm^2$.

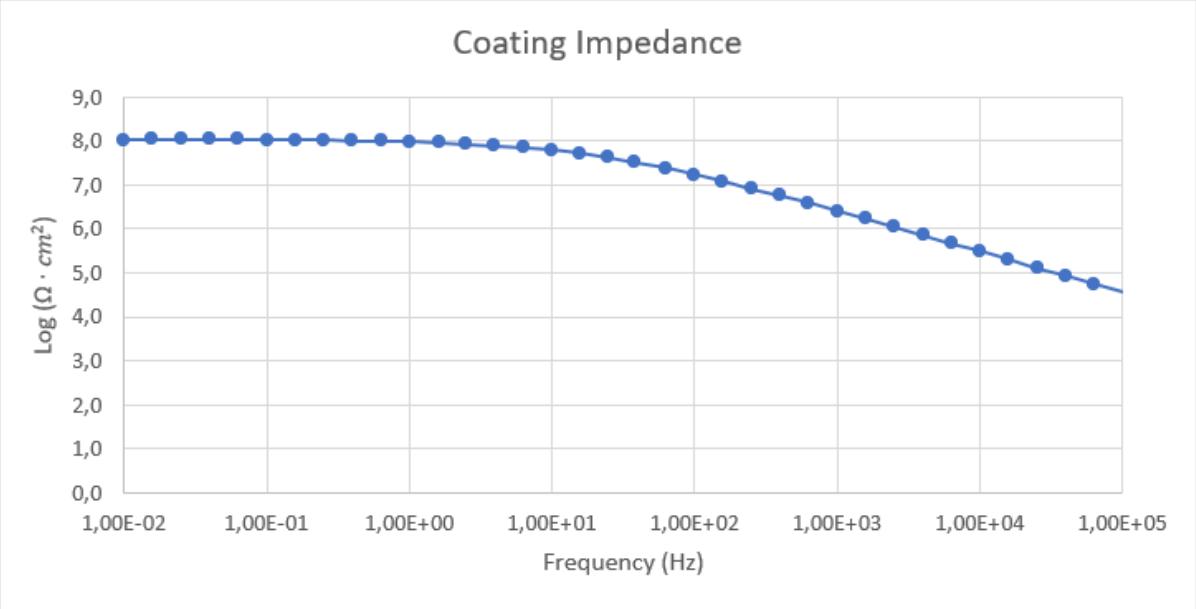

Figure 11: The impedance spectrum of an organic coating displayed in a Bode plot.

3 Experimental

3.1 Coating Systems

Coating samples were provided by Jotun. The different systems seen in Figure 12 were prepared on carbon steel panels by Jotun. All coating products tested are anonymized in this report. Notably, the stated film thickness is nominal (NFT). Measured dry film thickness (DFT) was up to 25% higher for each specimen. A full description of DFT for each coating sample and a description of each parallel tested can be found in the appendix. Table 2 gives a description of the coatings as well as existing test results.

Table 2: Panel description of products received from Jotun with anonymized names. Testing of T_g was conducted by Jotun, using differential scanning calorimetry (DSC). CD testing was conducted by Jotun or externally by a third-party laboratory and were listed in equivalent circle diameter (ECD).

Coating	A	B	C	D	E	F
Number of panels	5	5	4	4	3	3
Number of coats	1	1	2	2	1	1
NFT	180 µm	180 µm	350 µm	350 µm	250 µm	250 µm
Aluminium Pigmented	Yes	No	Yes	No	Yes	Yes
Solids by volume	72%	97%	72%	97%	80%	82%
Generic Type	Solvent borne epoxy	Solvent free epoxy	Solvent borne epoxy	Solvent free epoxy	Solvent borne epoxymastic	Solvent borne epoxymastic
$T_{g,onset}$ (DSC)	-	~ 38°C	-	~ 38°C	~ 46°C	-
$T_{g,end}$ (DSC)	-	~ 47°C	-	~ 47°C	~ 62°C	-
$T_{g,Rev}$ (DSC)	-	~ 44°C	-	~ 44°C	~ 48°C	-
T_g-region	-	9°C	-	9°C	16°C	-
ASTM G8 (1 month)	ECD 12.5 mm	ECD 7.9 mm		ECD 7.8 mm	ECD 9.7 mm	ECD 9.5 mm
ISO 15711 (6 months)		ECD 0 mm	ECD 12.7 mm	ECD 0 mm		ECD 15.7 mm

What is referred to as coating C and D in Table 2, were panels with two coats of the same product as coating A and B, respectively. The appearance of the panels before testing is shown in Figure 12.

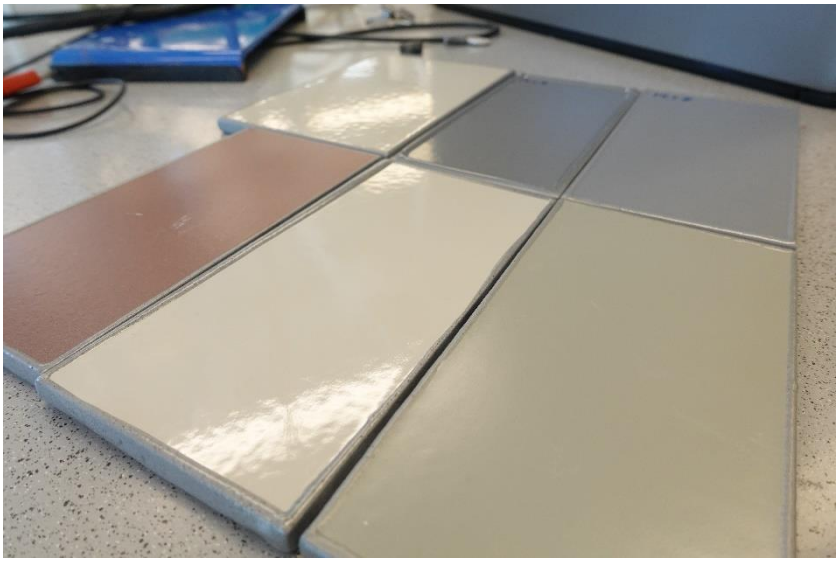

Figure 12: Six different coating systems that were tested. All provided by Jotun.

3.2 Testing Method

3.2.1 Setup

An electrochemical cell was prepared for the coating samples investigated (Table 2). The empty cell is shown in Figure 13, as it was prepared to attach coating samples. A platinum counter electrode had been placed in the bottom of the cell. The cell had six holes that could be covered with one coating sample each.

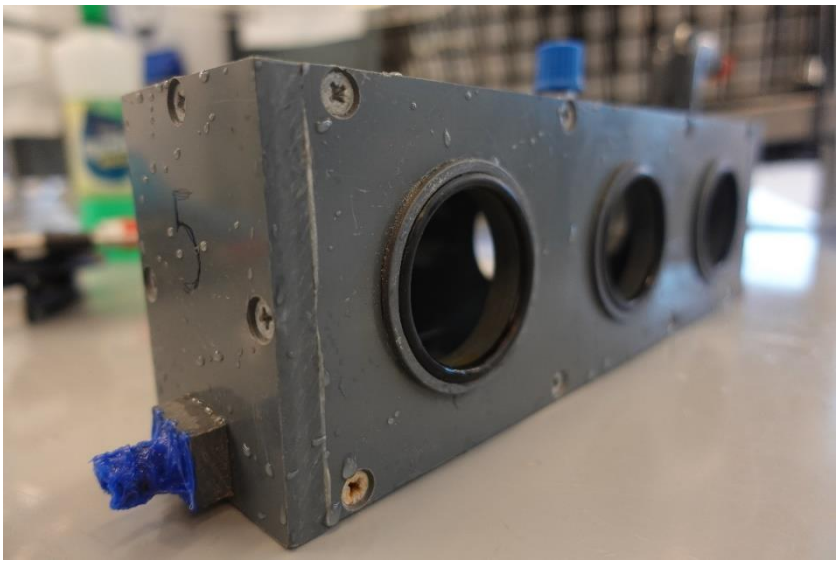

Figure 13: Empty electrochemical cell fitted with O-rings and platinum counter electrode.

The coating samples were fitted to the cell with clamps, seen in Figure 14. This is referred to as a parallel. The clamps also had the crucial function of keeping the cell tight so that it could be filled with an electrolyte. The electrolyte used was 3.5 wt% $NaCl$. A new electrolyte was prepared and added to the electrochemical cell for each parallel that was tested. All samples were exposed to the electrolyte for a minimum of 48 hours before testing was conducted to saturate the coating samples. The area of the exposed coating was 19.64 cm^2 per coating sample.

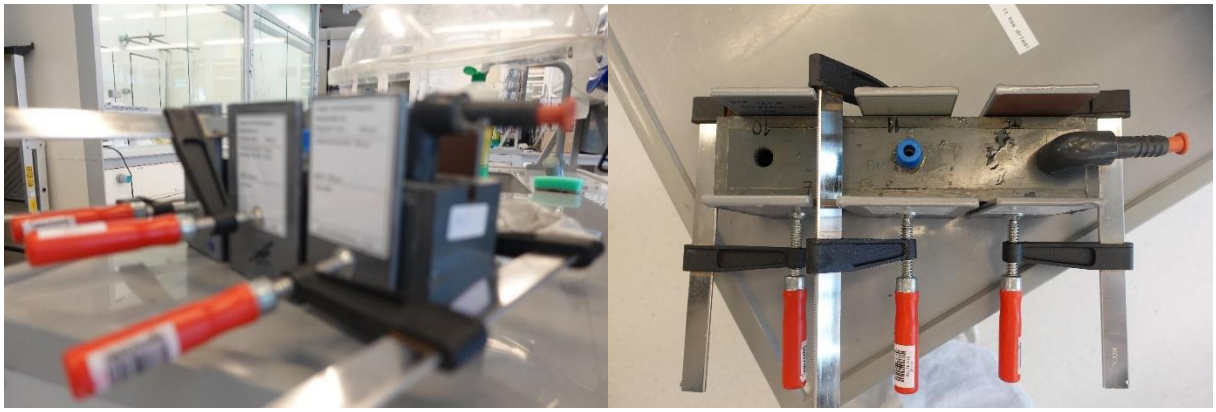

Figure 14: Coating samples fitted to the electrochemical cell. The illustration to the left is blurred to anonymize product names.

The top corner of each coating sample was grinded down to the bare steel so that the working cell cable could be attached to it.

The tests were conducted with an $Ag/AgCl$ reference electrode placed directly into the electrochemical cell. The $Ag/AgCl$ reference electrode was preferred as it can be used in electrolyte up to 90℃, while an SCE electrode would be limited to 60℃ [33].

A Gamry Interface 1010E potentiostat was used to conduct potentiostatic EIS on the coating samples. When measuring impedance at low frequencies with low current, electrical noise is a common issue that can affect the quality of the results [34]. Several measures were taken to reduce the noise. Original Gamry cell cables are claimed to have great protection against noise infiltration. This is allegedly partly achieved by a reproducible shielding around cell cables and an additional twisting of the cables [34]. Replaceable coaxial cables were connected on the other end of the connection box illustrated in Figure 15, with the purpose of entering a heat cabinet (see Figure 16) where the test cell was exposed to specific temperatures. The connection box was used to minimize electric noise by acting as a Faraday's cage.

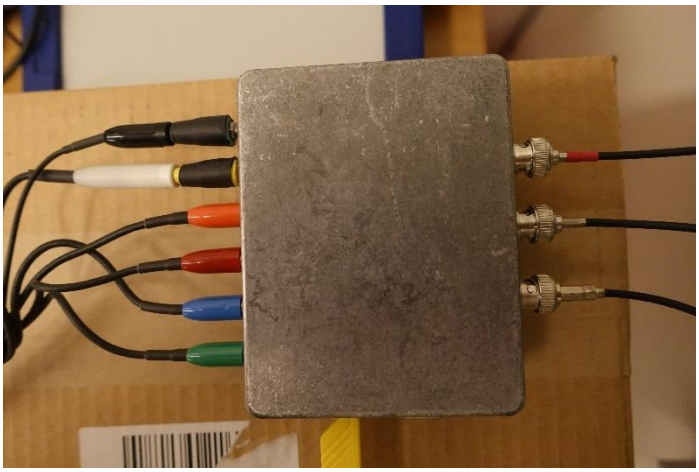

Figure 15: Protected connection box between original cables (left) and coaxial cables to the electrochemical cell (right).

The test setup seen in Figure 16 was developed for routinely usage. It features the electrochemical cell fitted with coating samples and coaxial cables inside the oven. The Gamry Interface1010E instrument was chassis grounded during the experiments to lower the noise.

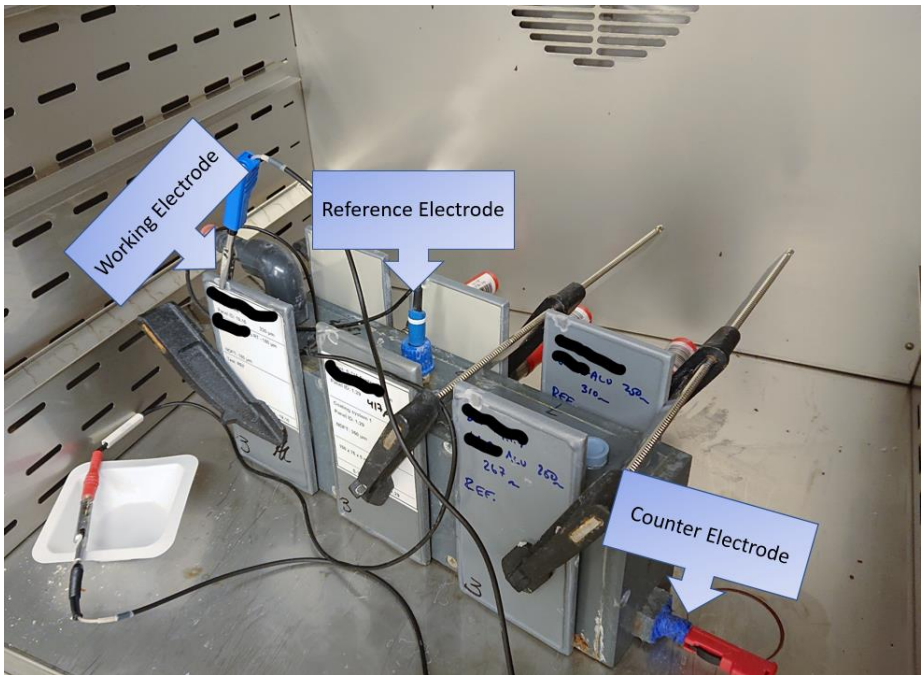

Figure 16: Test setup

3.2.2 EIS Measurement and Procedure

A cathodic potential was achieved by applying a sinusoidal voltage of -400 mV vs Ag/AgCl to the working electrode (coating sample). The impedance spectra were recorded in the frequency range of 10 mHz to 100 kHz. The AC voltage (amplitude of the AC signal) was set to 30 mV *RMS*.

Impedance was measured at temperatures ranging from 25°C to 70°C. All samples were measured at 25°C before the electrochemical cell was heated. The EIS measurements were conducted in a closed heating cabinet (appearing in Figure 16) to maintain a stable temperature. The temperature of the electrolyte in the electrochemical cell was measured with a thermometer before and during testing to confirm stable environmental conditions. A second thermometer was used to measure the electrolyte temperature during the testing of parallel 1 to ensure that the first thermometer was in reliable. No deviation was seen between the two thermometers.

Initially, it was planned to heat all coating samples from 25°C to 60°C with the aim of investigating the temperature dependence of impedance. It was, however, decided to investigate the effect of thermal cycling on impedance also. Thermal cycling schemes were

gradually developed during the experimental phase. The testing parallels were subjected to cyclic heating and EIS, specified in the schematic of thermal cycling displayed in Figure 17-Figure 19. However, parallel 1 and 2 were removed from the cell and dried after the initial heating cycle from 25°C to 60°C seen in Figure 17, then reattached after almost two weeks and exposed to the electrolyte for 48 hours before the thermal cycle was continued. Parallel 3, 4 and 5 were tested continuously without ever being removed from the cell.

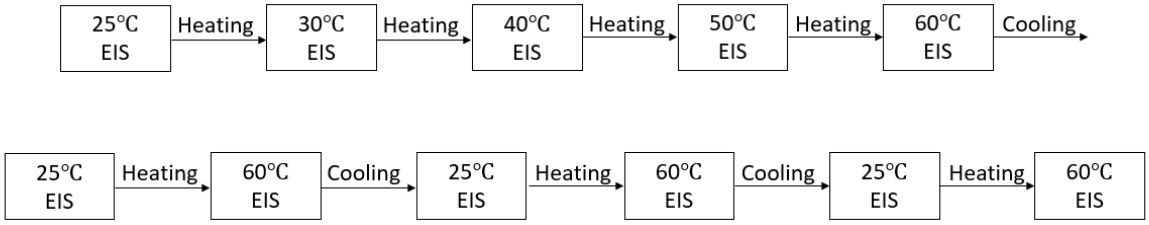

Figure 17: Thermal cycle scheme 1. Conducted on parallel 1 and 2.

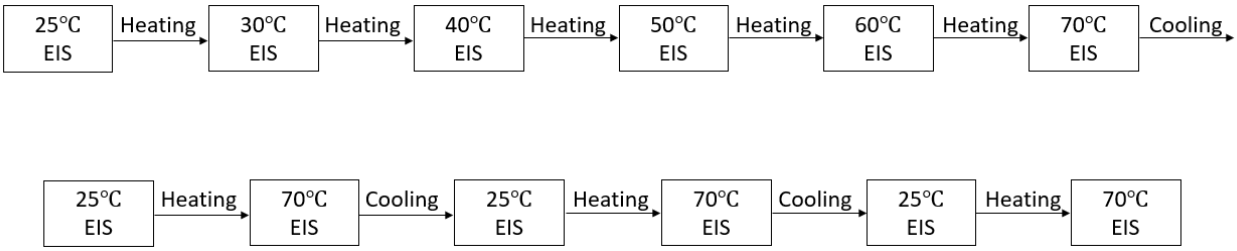

Figure 18: Thermal cycle scheme 2. Conducted on parallel 3.

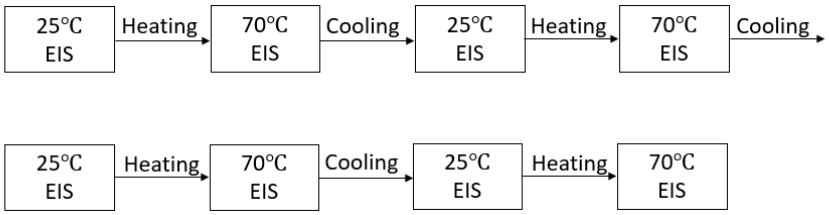

Figure 19: Thermal cycle scheme 3. Conducted on parallel 4 and 5.

4 Results

The results presented in this section show the temperature dependence of impedance and the effect of thermal cycling on coating samples. The 10 mHz measuring is referred to as the impedance of a coating and is always assumed to be indicating the R_p of the coating that was tested. Low noise was observed in the recorded impedance data, as shown in Figure 20. Therefore, the exact measured value at 10 mHz was presented as the impedance of each coating sample.

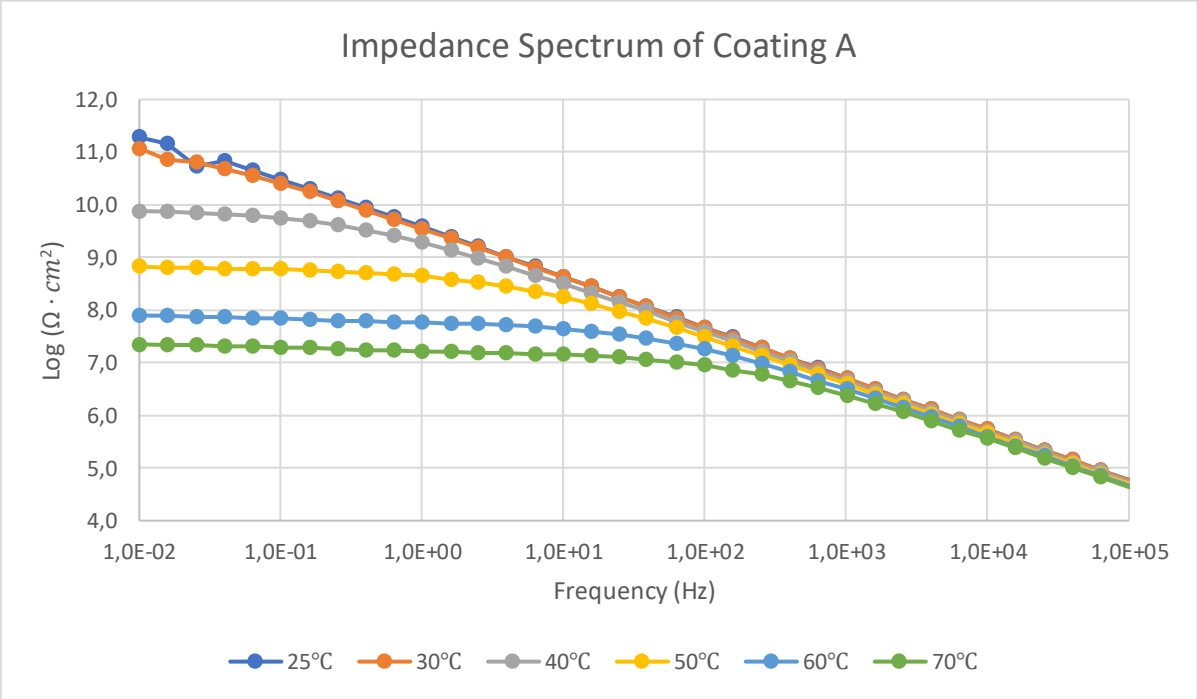

Figure 20: A Bode plot showing the impedance spectrum of coating A with various frequencies at temperatures ranging from 25°C to 70°C.

The instrument producer Gamry states that the potentiostat used in these experiments (1010E) has an impedance measuring accuracy greater than 99% when the impedance measured is below 10^{10} Ω and above 0.001 Ω. The impedance measured on some of the coating samples at 25°C was higher than the accurate reading range of the instrument. It can only be certain that these measurements were above 10^{10} Ω.

All coating samples were visually inspected after testing. No sign of coating degradation was observed on any samples.

4.1 Temperature Dependence of Impedance

The coatings were subjected to a gradual increase in temperatures from 25°C to 70°C. This was the first cycle of heating according to the thermal cycle schemes presented in Figure 17-Figure 19.

The impedance of coating A measured at 25°C was over $10^{10}\ \Omega \cdot cm^2$. A decrease in impedance was seen as the temperature increased, which is shown in Figure 21. The greatest decrease was seen between 30°C and 40°C. At the temperature of 70°C, the impedance of coating A was over $10^{7}\ \Omega \cdot cm^2$. The impedance of coating A, parallel 2 at 30°C was removed due to a fault in the measuring.

The impedance of coating B measured at 25°C was over $10^{10}\ \Omega \cdot cm^2$. A decrease in impedance was seen as the temperature increased, which is shown in Figure 22. The greatest decrease was seen between 30°C and 40°C. At the temperature of 70°C, the measured impedance of coating B was slightly under $10^{7}\ \Omega \cdot cm^2$.

The impedance of coating C measured at 25°C was over $10^{10}\ \Omega \cdot cm^2$. A decrease in impedance was seen as the temperature increased, which is shown in Figure 23. The greatest decrease was seen between 30°C and 40°C. At the temperature of 70°C, the measured impedance of coating C was slightly under and slightly over $10^{8}\ \Omega \cdot cm^2$. Coating C was the coating that retained the highest value of impedance measured at 70°C.

The impedance of coating D measured at 25°C was over $10^{10}\ \Omega \cdot cm^2$. A decrease in impedance was seen as the temperature increased, which is shown in Figure 24. The greatest decrease was seen between 30°C and 40°C. At the temperature of 70°C, the measured impedance of coating D was slightly under and slightly over $10^{7}\ \Omega \cdot cm^2$.

The impedance of coating E measured at 25°C varied from slightly under $10^{9}\ \Omega \cdot cm^2$ to over $10^{10}\ \Omega \cdot cm^2$. A decrease in impedance was seen as the temperature increased, which is

shown in Figure 25. The greatest decrease was seen between 30°C and 40°C. At the temperature of 70°C, the impedance of coating E was slightly under $10^8\ \Omega \cdot cm^2$.

The impedance of coating F measured at 25°C varied from slightly under and over $10^9\ \Omega \cdot cm^2$ to over $10^{10}\ \Omega \cdot cm^2$. A decrease in impedance was seen as the temperature increased, which is shown in Figure 26. The greatest decrease was seen between 25°C and 30°C. However, a large variation in results was observed. At the temperature of 70°C, the measured impedance of coating F was close to $10^7\ \Omega \cdot cm^2$.

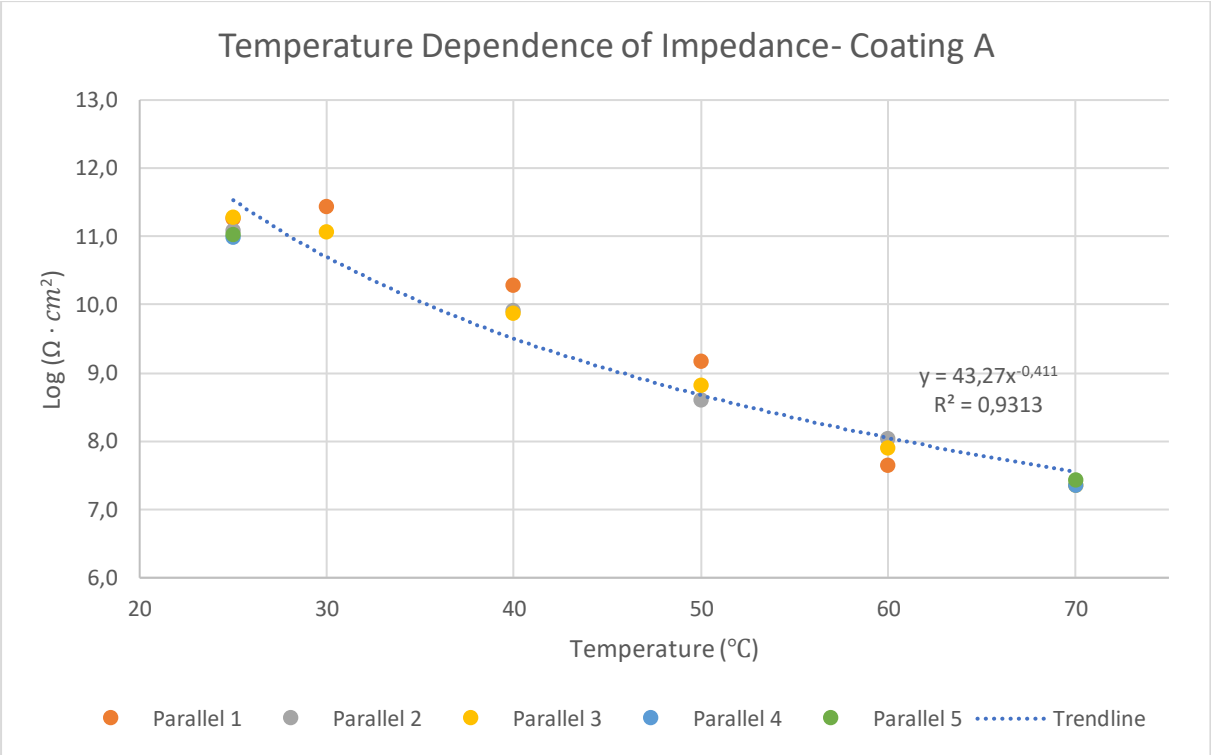

Figure 21: The temperature dependent impedance of coating A. NDFT: 180 µm. Experimental conditions: Exposed to water containing 3.5% NaCl for minimum two days at room temperature before testing. Applied potential during testing: -400 mV vs Ag/AgCl.

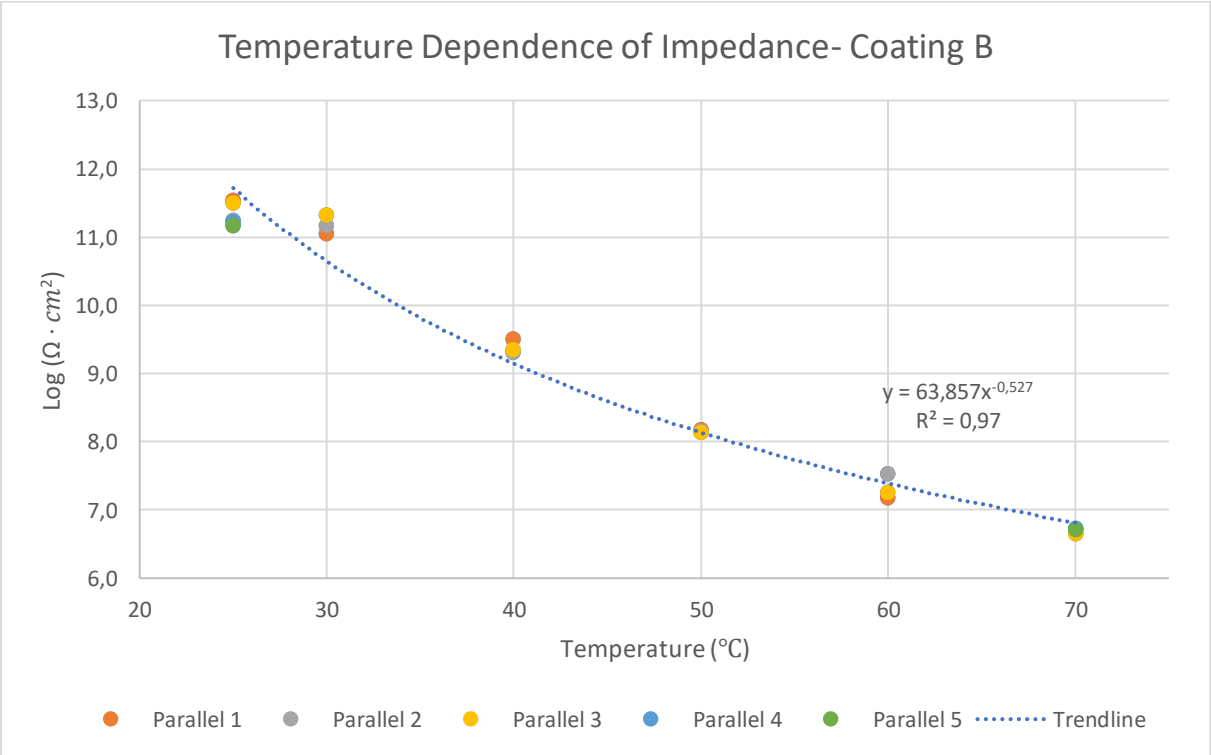

Figure 22: The temperature dependent impedance of coating B. NDFT: 180 µm. Experimental conditions: Exposed to water containing 3.5% NaCl for minimum two days at room temperature before testing. Applied potential during testing: -400 mV vs Ag/AgCl.

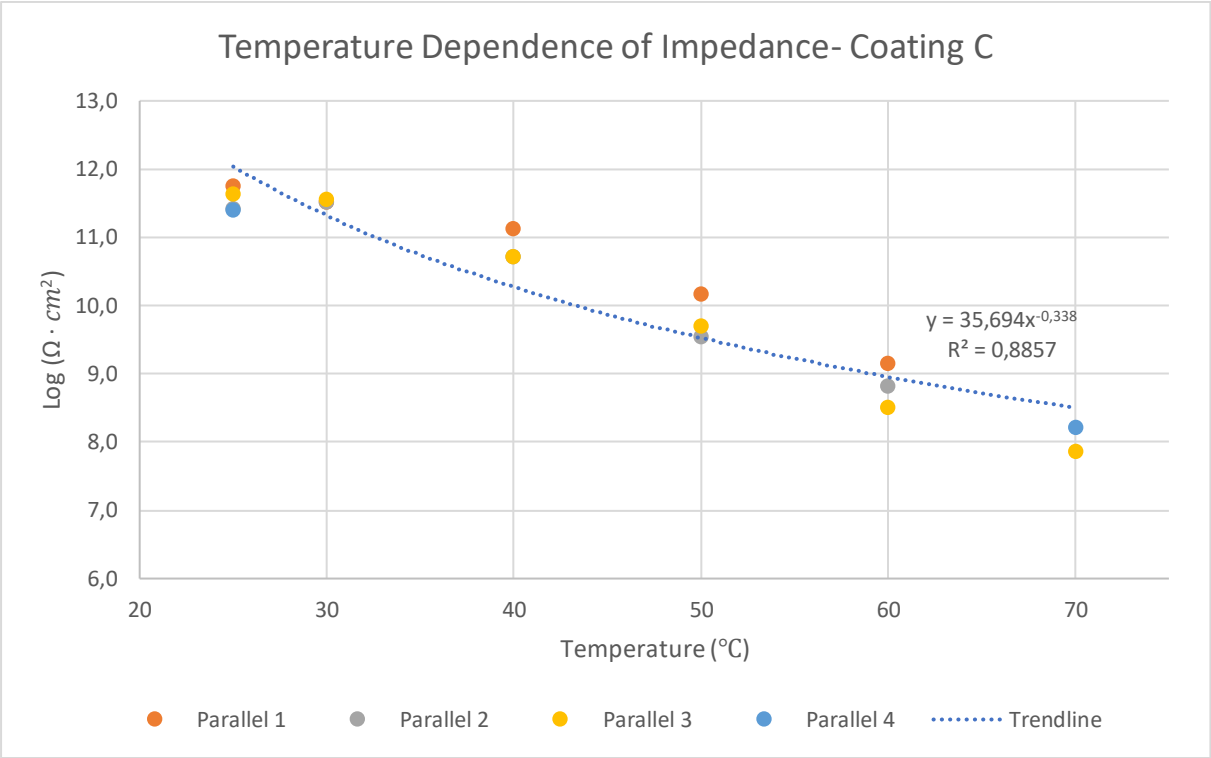

Figure 23: The temperature dependent impedance of coating C. NDFT: 350 µm. Experimental conditions: Exposed to water containing 3.5% NaCl for minimum two days at room temperature before testing. Applied potential during testing: -400 mV vs Ag/AgCl.

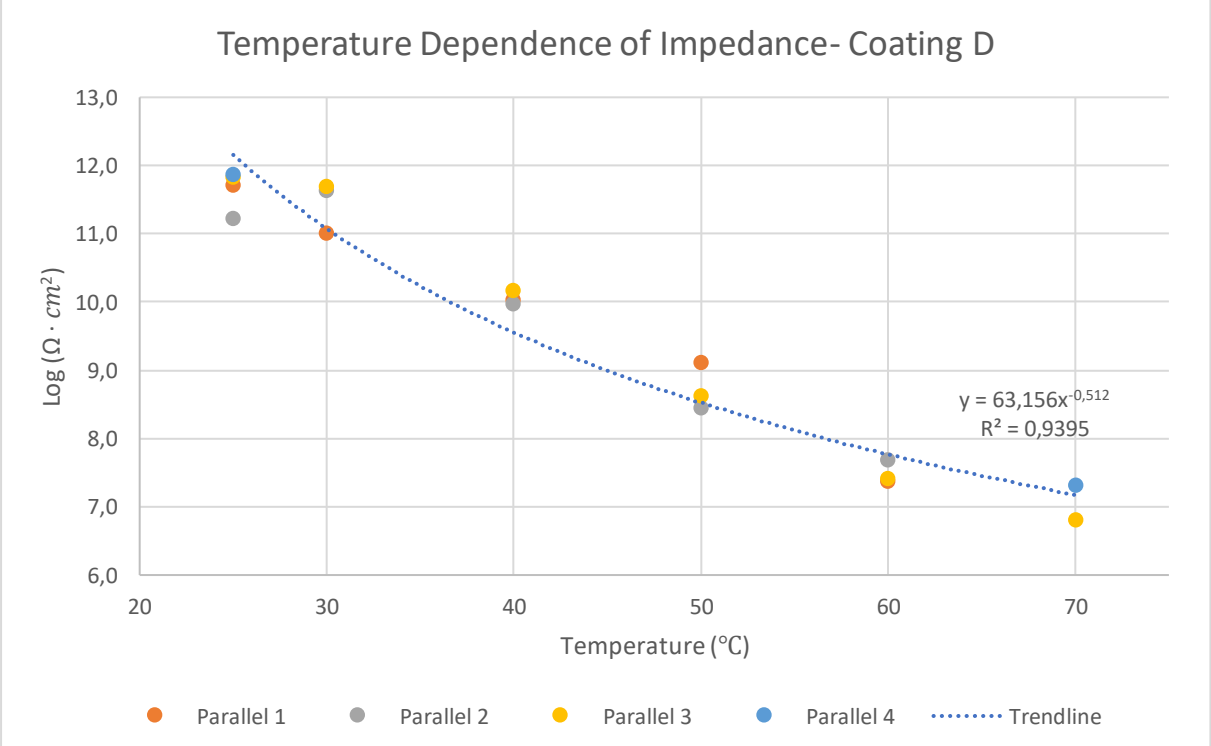

Figure 24: The temperature dependent impedance of coating D. NDFT: 350 µm. Experimental conditions: Exposed to water containing 3.5% NaCl for minimum two days at room temperature before testing. Applied potential during testing: -400 mV vs Ag/AgCl.

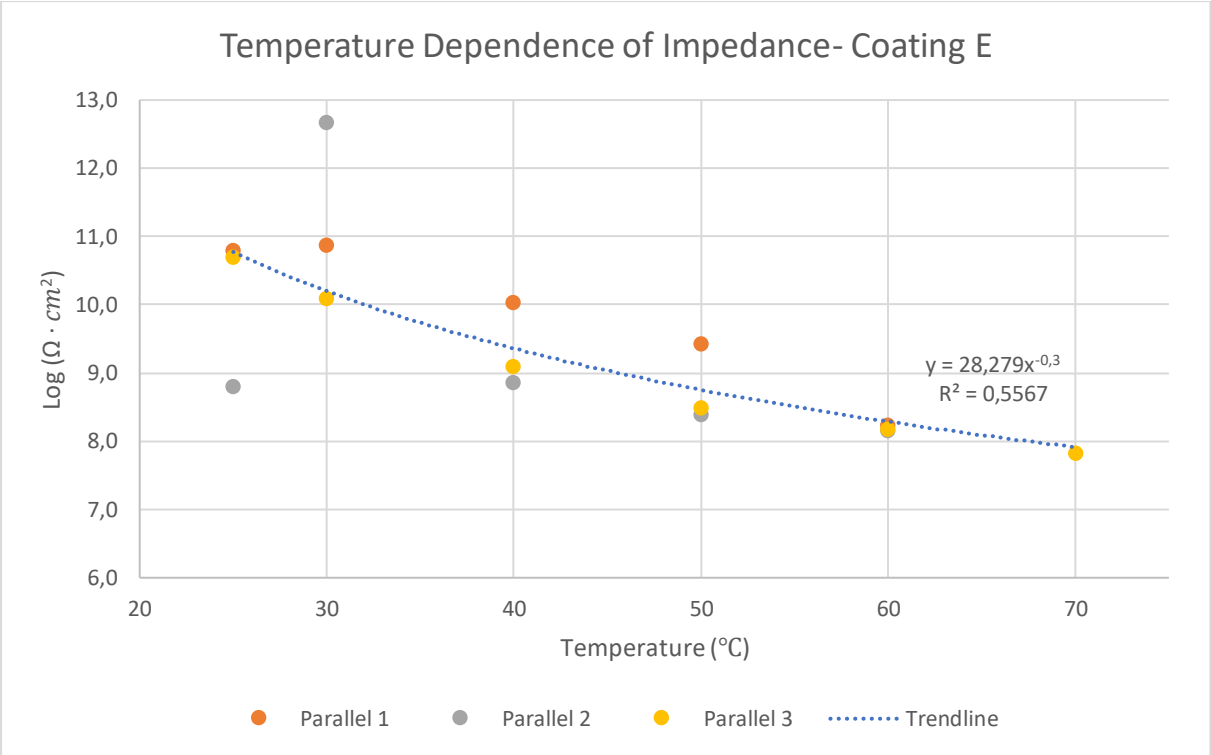

Figure 25: The temperature dependent impedance of coating E. NDFT: 250 µm. Experimental conditions: Exposed to water containing 3.5% NaCl for minimum two days at room temperature before testing. Applied potential during testing: -400 mV vs Ag/AgCl.

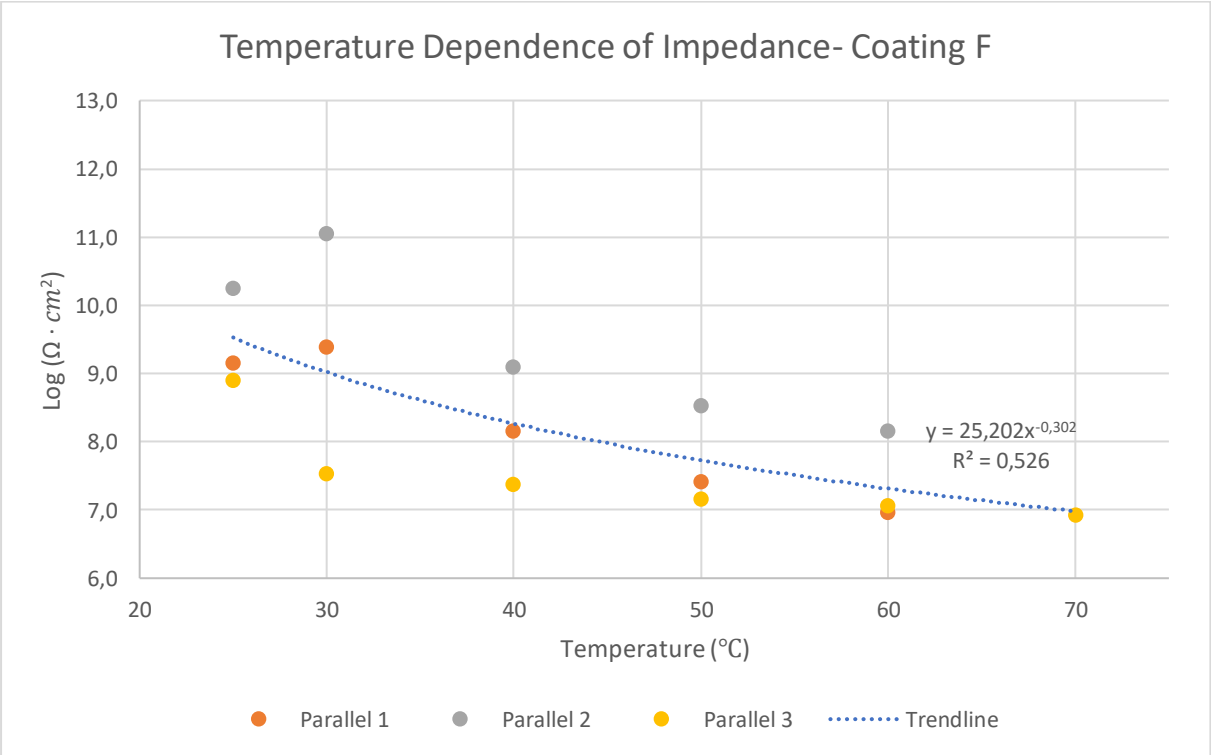

Figure 26: The temperature dependent impedance of coating F. NDFT: 250 µm. Experimental conditions: Exposed to water containing 3.5% NaCl for minimum two days at room temperature before testing. Applied potential du during testing: -400 mV vs Ag/AgCl.

4.2 Thermal Cycling

Results from the thermal cycling of the coatings according to the thermal cycling schemes shown in Figure 17- Figure 19, are presented here. Only the impedance measured at 25°C is presented, as the aim was to investigate the reversibility of impedance for each coating.

The impedance measured on coating A at 25°C in the first thermal cycle was over $10^{10}\ \Omega \cdot cm^2$. Coating A showed a decrease in impedance during thermal cycling, as shown in Figure 27. The greatest decrease in impedance was observed after one cycle of heating. In the fourth thermal cycle, only one coating sample had an impedance of less than $10^{10}\ \Omega \cdot cm^2$. The impedance of coating A, parallel 5 in the third thermal cycle was removed due to a fault in the measuring.

The impedance measured on coating B at 25°C in the first thermal cycle was over $10^{10}\ \Omega \cdot cm^2$. Coating B showed a decrease in impedance during thermal cycling, as shown in Figure 28. The greatest decrease in impedance was observed after one cycle of heating. All coating samples displayed an impedance of over $10^{10}\ \Omega \cdot cm^2$ in the fourth thermal cycle.

The impedance measured on coating C at 25°C in the first thermal cycle was over $10^{10}\ \Omega \cdot cm^2$. Coating C showed a decrease in impedance during thermal cycling, as shown in Figure 29. The greatest decrease in impedance was observed after one cycle of heating. All coating samples displayed an impedance of over $10^{10}\ \Omega \cdot cm^2$ in the fourth thermal cycle.

The impedance measured on coating D at 25°C in the first thermal cycle was over $10^{10}\ \Omega \cdot cm^2$. Coating D showed a decrease in impedance during thermal cycling, as shown in Figure 30. The greatest decrease in impedance was observed after one cycle of heating. All coating samples displayed an impedance of over $10^{10}\ \Omega \cdot cm^2$ in the fourth thermal cycle.

The impedance measured on coating E at 25°C in the first thermal cycle was over $10^{10}\ \Omega \cdot cm^2$ except one sample, which measured under $10^{9}\ \Omega \cdot cm^2$. This sample displayed an increase in impedance during thermal cycling, as shown in Figure 31. All other samples

displayed an insignificant change in impedance during thermal cycling. All coating samples displayed an impedance of over $10^{10}\ \Omega \cdot cm^2$ in the fourth thermal cycle.

The impedance measured on coating F at 25°C in the first thermal cycle varied, as shown in Figure 32. Two of the samples displayed an impedance of slightly under and over $10^{9}\ \Omega \cdot cm^2$, while a third sample displayed an impedance of over $10^{10}\ \Omega \cdot cm^2$. The greatest decrease in impedance was observed after one cycle of heating for the two samples with lowest initial impedance, while the sample with the highest initial impedance retained its impedance during thermal cycling. The impedance measured on parallel 1, 2 and 3 in the fourth thermal cycle was over $10^{8}\ \Omega \cdot cm^2$, $10^{10}\ \Omega \cdot cm^2$ and $10^{7}\ \Omega \cdot cm^2$, respectively.

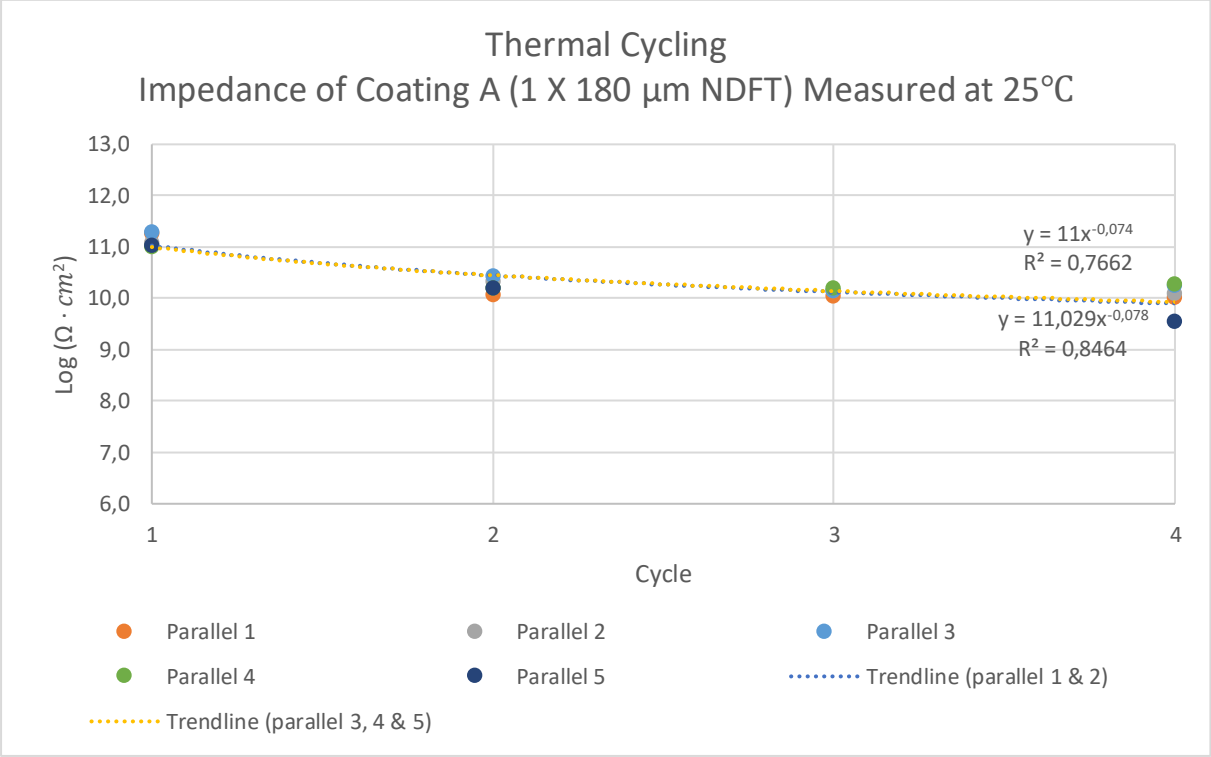

Figure 27: The impedance of coating A measured at 10 mHz. Experimental conditions: Exposed to water containing 3.5% NaCl for minimum two days at room temperature before testing. Applied potential during testing: -400 mV vs Ag/AgCl.

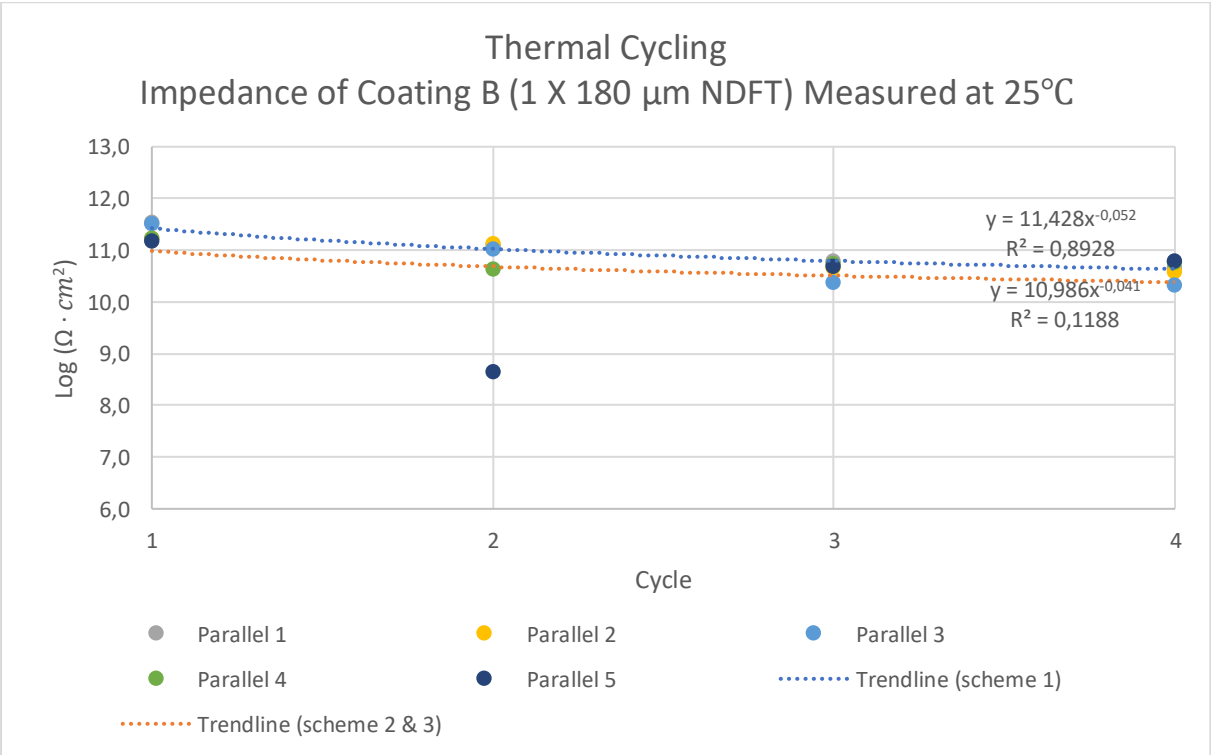

Figure 28: The impedance of coating B measured at 10 mHz. Experimental conditions: Exposed to water containing 3.5% NaCl for minimum two days at room temperature before testing. Applied potential during testing: -400 mV vs Ag/AgCl.

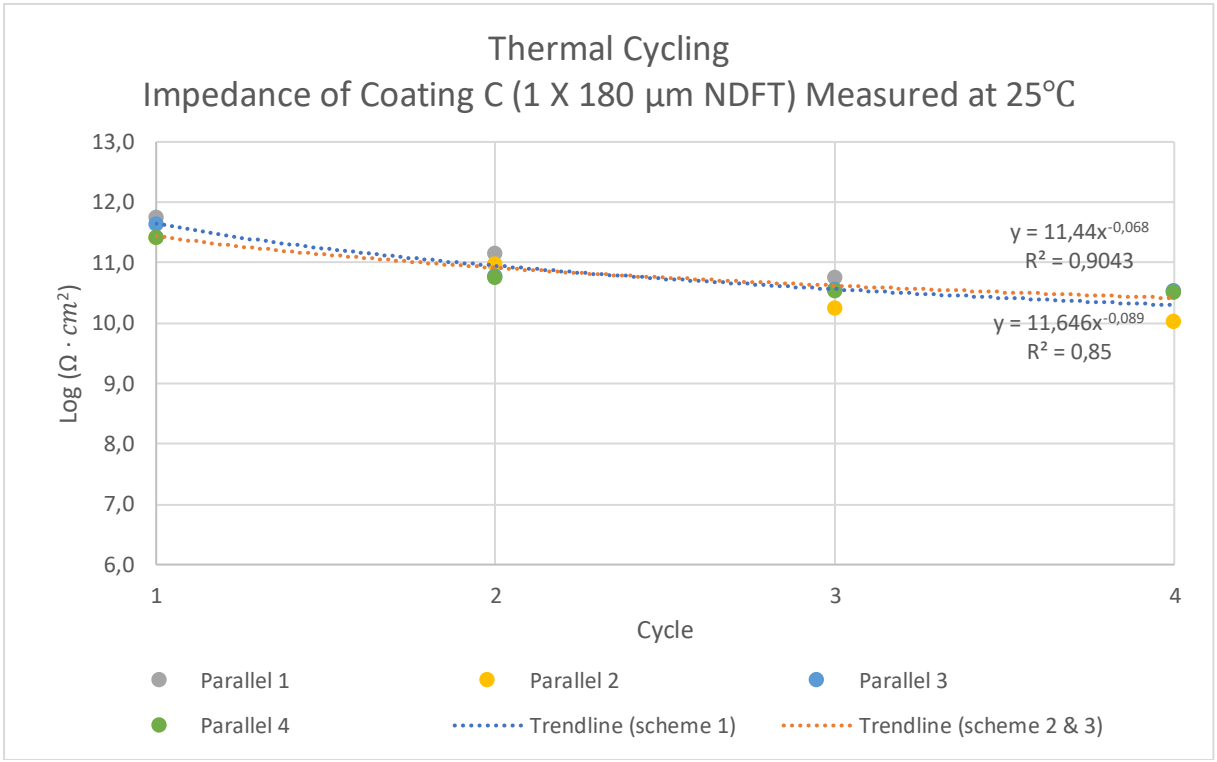

Figure 29: The impedance of coating C measured at 10 mHz. Experimental conditions: Exposed to water containing 3.5% NaCl for minimum two days at room temperature before testing. Applied potential during testing: -400 mV vs Ag/AgCl.

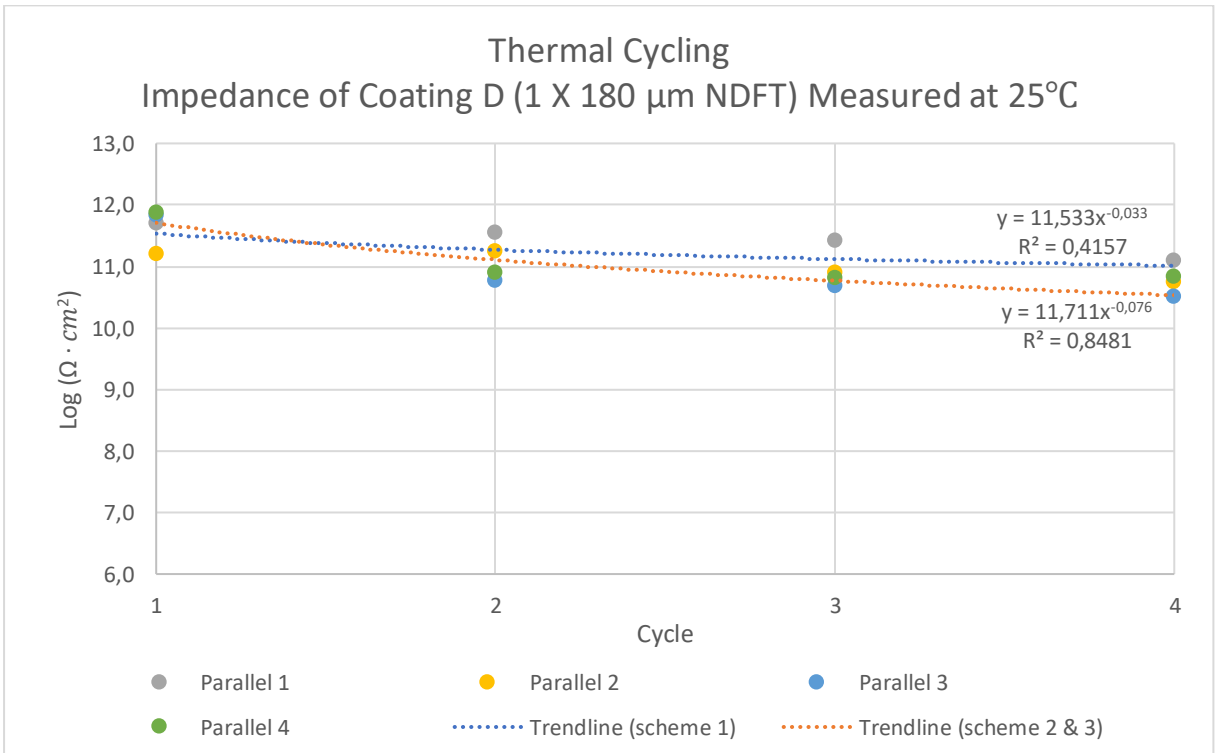

Figure 30: The impedance of coating D measured at 10 mHz. Experimental conditions: Exposed to water containing 3.5% NaCl for minimum two days at room temperature before testing. Applied potential during testing: -400 mV vs Ag/AgCl.

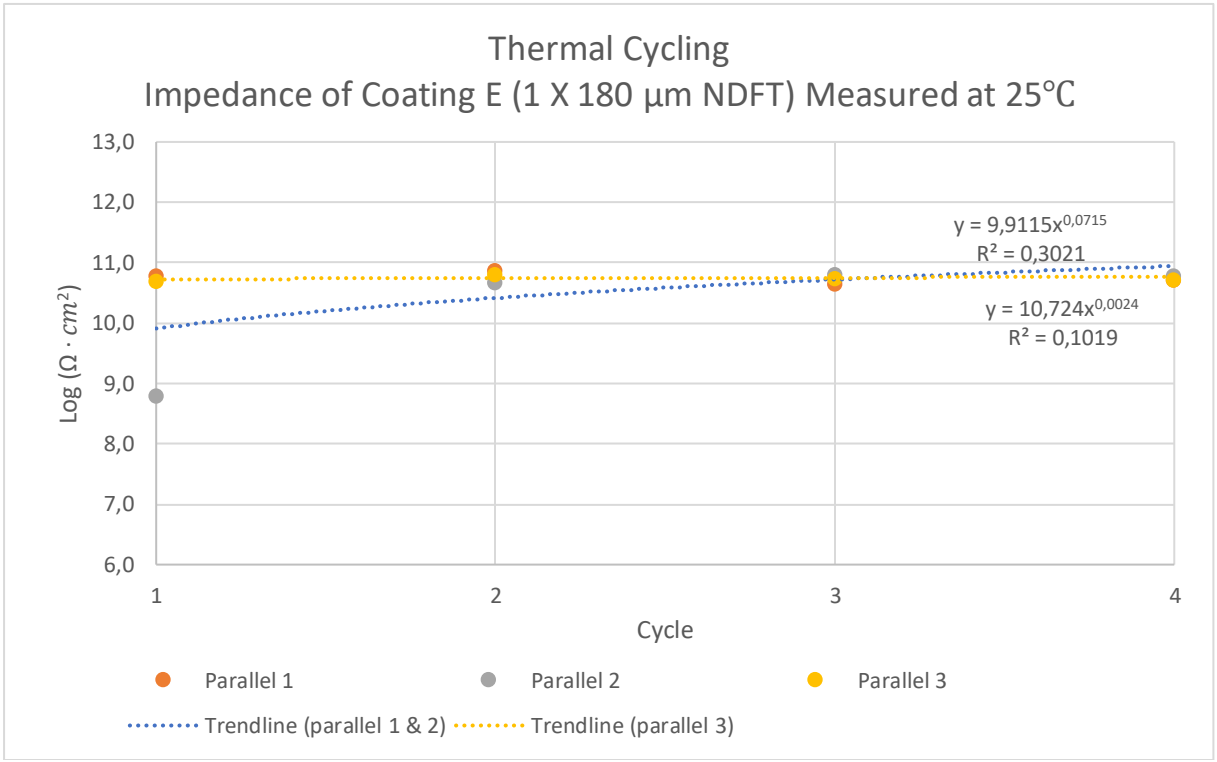

Figure 31: The impedance of coating E measured at 10 mHz. Experimental conditions: Exposed to water containing 3.5% NaCl for minimum two days at room temperature before testing. Applied potential during testing: -400 mV vs Ag/AgCl.

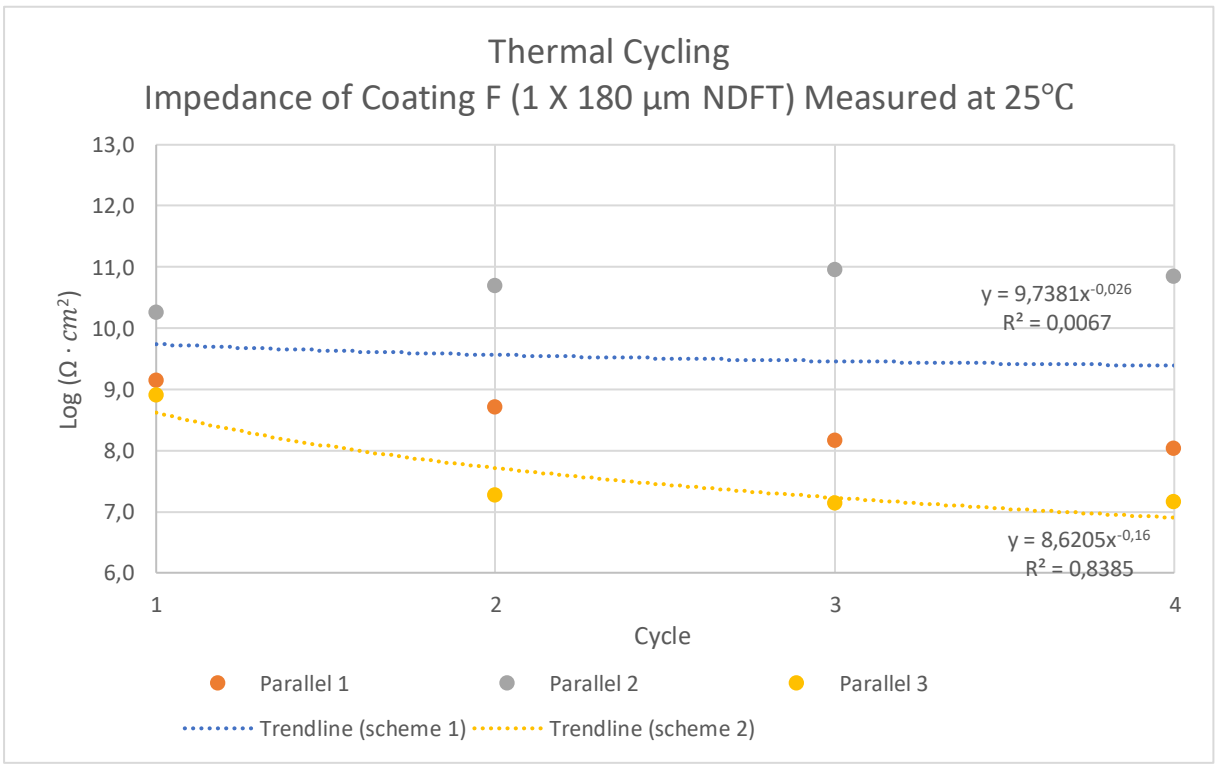

Figure 32: The impedance of coating F measured at 10 mHz. Experimental conditions: Exposed to water containing 3.5% NaCl for minimum two days at room temperature before testing. Applied potential during testing: -400 mV vs Ag/AgCl.

5 Discussion

The initial impedance measured on all coatings at 25°C was over $10^9\ \Omega \cdot cm^2$, where durable barrier properties are expected [7, 12, 14, 15]. The different effects that were observed during testing of the coatings are discussed in this section.

The experiments were not conducted coherently on parallel 1 and parallel 2. Though this was not an optimal testing procedure, no effect of drying the samples, and then continuing measurements were observed. No published work could be found that suggested drying the samples and re-exposing them to an electrolyte would affect the impedance of the coatings. Therefore, the results of all parallels are considered representative of the effect of temperature and thermal cycling on coating impedance.

5.1 Effect of Temperature on Impedance

The measured impedance decreased with increased temperature on all coatings.

Film thickness and number of coats affected the temperature's effect on impedance. Coating C performed better than coating A, and coating D performed better than coating B with increase in temperature. Higher impedance was observed for the coatings with higher film thickness and two coats. The same effect of film thickness was observed by Bierwagen et. al. [14] and Shreepathi [20]. There was not found any published work that indicated an effect of number of coats on impedance. The increased impedance that was observed was likely due to the higher film thickness. However, an effect of two coats cannot be excluded. As shown in Figure 21 and Figure 23, the impedance measured at 25°C was over $10^{10}\ \Omega \cdot cm^2$ for both coating C and coating A. The impedance measured on coating C was less affected by temperature and displayed a higher impedance measured at 70°C. As shown in Figure 22 and Figure 24, the same trend was observed for coating D and coating B, where the impedance measured at 25°C was over $10^{10}\ \Omega \cdot cm^2$. As the temperature increased, a lower decrease in impedance was observed for coating D compared to coating B.

Coating E and coating D were two different coatings with respect to number of coats, film thickness, T_g-region and aluminium pigments. These coatings are interesting to compare as they were affected differently by temperature. Coating E displayed less effect of temperature on its impedance than coating D, despite having lower film thickness and one coat, shown in Figure 24 and Figure 25. The T_g-region of coating E was higher than that of coating D and coating B, as listed in Table 2. As studies suggest [20, 27], coatings will display significant decrease in impedance as they are immersed and exposed to temperatures higher than $T_{g,onset}$. Also, the T_g-region of coatings have been shown to decrease as an effect of immersion [21]. It could therefore be expected that the impedance of coating B and coating D were affected more by temperature than coating E, as they were exposed to temperatures above the T_g-region. A variation between the samples was observed for the impedance measured on coating F at 25°C, shown in Figure 26. The impedance of coating F showed an effect of temperature that was similar to coating E. However, the sample in parallel 3 had an initial impedance of slightly under $10^9\ \Omega \cdot cm^2$ at 25°C and slightly under $10^7\ \Omega \cdot cm^2$ at 70°C.

If the temperature dependence of impedance for the coatings (Figure 21-Figure 26) is assumed, the trendlines can be extrapolated towards higher temperatures, as shown in Figure 33. The extrapolated temperature dependence can be used to indicate the coating properties at higher temperatures. When coatings have impedance under $10^6\ \Omega \cdot cm^2$, low barrier properties and less protective behavior is displayed as a result of increasing passage of ionic charges through the coating [12, 15]. Considering the extrapolation, an impedance under $10^6\ \Omega \cdot cm^2$ can be expected by coating B at around 90°C and coating D at around 100°C. Coating A and coating F are likely to be in the range between $10^6\ \Omega \cdot cm^2$ and $10^7\ \Omega \cdot cm^2$ at 100°C, where they may provide fairly working protection of the substrate, but with some effect on the impedance by conductive pathways [7, 12]. It is fair to assume that coating C and coating E will display an impedance of $10^7\ \Omega \cdot cm^2$ or higher at 100°C and may even be providing some protection of the substrate at 120°C. Another interesting difference between the coatings is shown in Figure 33. It can be observed that the coating product A/C demonstrates consistently higher impedance than the coating product B/D with increased temperature. This effect is apparent already at around 50°C, where coating A (180 µm NDFT) displays higher impedance than coating D (350 µm NDFT). This may indicate that the temperature dependence of coating B and coating D is not outweighed by an increase in film thickness. If so, the barrier property of the coating product B/D may not be significantly improved by

increased DFT. This could indicate that the coating product B/D is inferior to coating product A/C at higher temperatures, regardless of DFT employed.

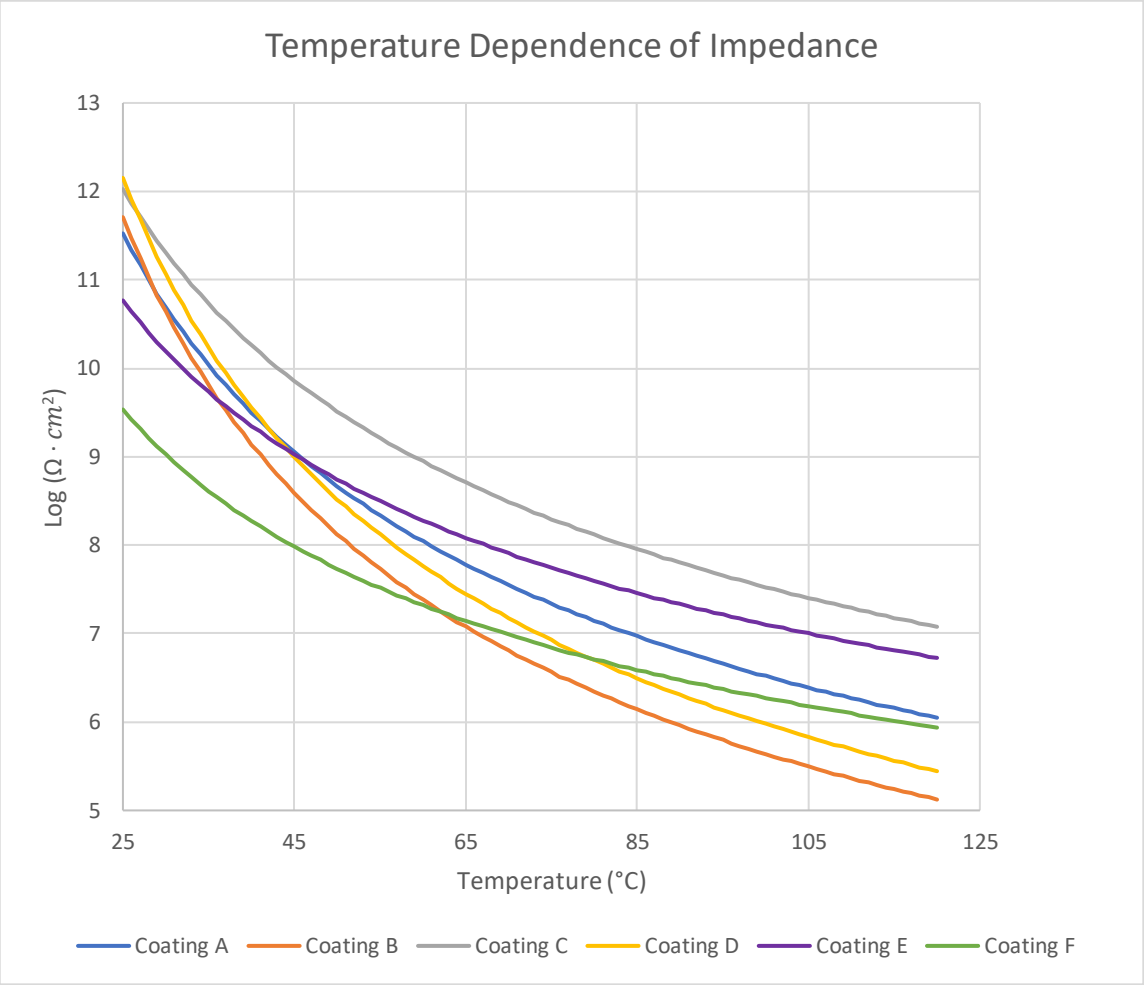

Figure 33: The extrapolated trendlines of all coatings tested in the temperature dependence of impedance experiments.

5.2 Effect of Thermal Cycling on Impedance

All coatings except coating E and coating F displayed a permanent decrease in impedance as an effect of thermal cycling. A significant difference of thermal cycling to 70°C compared to 60°C was not observed. Increased impedance from thermal cycling is, however, an effect that could have been observed. As the coatings were subjected to temperatures above their curing temperature in thermal cycling, a post-curing process with crosslinking could have taken place [35]. Higher cross-linked structure in epoxy coatings are characterized by increased low frequency impedance [36].

As shown in Figure 27- Figure 30, the effect of thermal cycling on coating A, B, C and D was an irreversible decrease in impedance for every cycle. The largest decrease was observed after the first cycle. An effect of film thickness or number of coats on the reversibility of impedance could not be observed for these coatings. These coatings retained impedance of over $10^9\ \Omega \cdot cm^2$ in the fourth thermal cycle. As the impedance of these coatings decreased as an effect of thermal cycling, it is likely that post-curing did not occur during heating. The decrease in impedance is likely to have been caused by a permanent opening of pores in the coating that act as a passage allowing transport of ions through the film, meaning less electrolytical resistance [12].

Two samples of coating E displayed reversible impedance in thermal cycling, shown in Figure 31. The sample of coating E in parallel 2 displayed a significant increase in impedance as an effect of thermal cycling. This was observed from the first to the second cycle, where the impedance went from slightly under $10^9\ \Omega \cdot cm^2$ to over $10^{10}\ \Omega \cdot cm^2$. The lower impedance measured in the first cycle could have been due to an experimental error since the effect in the second cycle is difficult to explain theoretically. A decrease of impedance on coating E could possibly be seen with more cycles at higher temperatures. However, Bierwagen et. al. [7] found epoxy coatings with lower film thickness to display small amounts of irreversibility of impedance as well, with similar thermal cycles spanning over eight days at higher temperatures (85°C).

Large variations in impedance from sample to sample was observed for coating F, shown in Figure 32. This may be attributed to imperfections in the coating samples that cause lower impedance, such as microcracks [37]. Parallel 3 that was cycled to 70°C displayed more irreversible impedance than the two samples that were cycled to 60°C. Not enough samples were tested to suggest that cycling of coating F to 70°C resulted in larger irreversibility of impedance. Also, the initial impedance measured on the sample of coating F in parallel 3 was lower than the two other samples of coating F, with an impedance of slightly under $10^9\ \Omega \cdot cm^2$. The sample of coating F in parallel 2 displayed a significant increase in impedance as an effect of thermal cycling and retained an impedance of over $10^{10}\ \Omega \cdot cm^2$ in both the first and the fourth cycle. This was displayed by both coating E and coating F in parallel 2, where a fault in the measuring or instruments were suspected for the first thermal cycle.

5.3 Effect of T_g on Reversibility of Impedance

As stated in Table 2, the T_g-region of coating B and coating D was significantly different than that of coating E. Therefore, it is interesting to compare these coatings. Thermal cycling had less effect on the impedance of coating E than coating D, despite having lower film thickness and a single coat. Coating E was the coating that displayed the most reversibility of impedance in thermal cycling. Coating E had a higher and larger T_g-region than coating B and coating D. This could have had a significant effect on the results in thermal cycling. Immersion and thermal cycling are factors that has been proven to decrease the T_g of some coatings [7], which can explain the fast decrease in impedance of coating B and coating D that was observed at temperatures over the $T_{g,onset}$ of the coatings stated in Table 2.

The permanent effect of decreased impedance from electrolyte exposure and thermal cycling can be observed when epoxy coatings are immersed and subjected to temperatures above the T_g-region for longer periods [21], as irreversible water uptake and swelling takes place [23]. This may be the explanation for the irreversibility of impedance observed in Figure 27- Figure 30. However, the irreversibility of impedance displayed by coating A, B, C and D could be considered as low because they retained an impedance of over $10^9\ \Omega \cdot cm^2$ in the fourth thermal cycle.

5.4 Correlation Between Impedance and CD

The experimental conditions that these coatings were subjected to are known to cause CD [3, 27]. No degradation of the coating samples was observed after any of the experiments. However, the testing was conducted over short time periods and the potential applied was less cathodically polarized compared to that of several studies on CD that have found significant degradation on epoxy coatings [5, 12, 20]. The results show that these coatings generally display impedance of over $10^9\ \Omega \cdot cm^2$ and low to insignificant irreversibility of impedance in thermal cycling. These characteristics are associated with durability and high resistance against CD [7]. The high bulk resistance of these coatings measured as impedance may be correlating to a high resistance on the interface between the coating and substrate. The driving force of CD is possibly cation migration under adhering coating driven by the potential gradient in the disbonding front [4]. If these coatings were damaged, the high resistance on

the substrate/coating interface could be limiting ionic migration under the adhering coating and therefore limit CD [17].

The recieved results from CD testing showed that all the coating systems displayed high resistance to CD at 23°C (see Table 2). However, coating B and coating D performed better than the other systems. These were also the coatings that displayed highest impedance in the first thermal cycle, shown in Figure 28 and Figure 30. There was not observed any other significant correlations between the effect of temperature on impedance or thermal cycling and the existing CD results of the coatings.

Three of the four aluminium pigmented coatings (A, C and E) displayed less effect of temperature on impedance than the two coatings without aluminium pigments (B and D). This is shown in Figure 21, Figure 23 and Figure 25 where the impedance of the aluminium pigmented coatings was higher at 70°C. An exception was observed in Figure 26 with coating F. Coating F was aluminium pigmented but displayed roughly the same impedance as coating B and coating D at 70°C (around $10^7\ \Omega \cdot cm^2$). Aluminium pigmented coatings are expected to have better resistance against CD [20]. However, no published work was found that suggested aluminium pigments affect impedance. Knudsen and Steinsmo [25] found indication that the effect aluminium pigments have on increased resistance to CD is due to chemical activity, and not electrolytical resistance. The existing results of CD testing on the coating systems (Table 2) showed that the two coatings without aluminium pigments performed better. This could suggest that the impedance of the coatings had a more significant effect on CD than aluminium pigments.

6 Conclusion

A test procedure was developed for routinely usage of EIS to assess coating properties and performance. Experiments were conducted on six coating systems to investigate the effects of temperature and thermal cycling on impedance. The results were compared to determine how the coating parameters influenced the impedance.

The following can be concluded:

- The impedance of all coatings decreased as an effect of increase in temperature.
- The impedance of coatings with higher film thickness decreased less with increase in temperature.
- The impedance of a coating with higher T_g-region was less affected by increase in temperature and displayed total reversible impedance in thermal cycling.
- Other coatings showed close to total reversible impedance in thermal cycling.
- There was a correlation between high impedance and resistance to CD.

6.1 Further Work

The effect of two coats on coating impedance was unclear. Thermal cycling tests can be conducted on samples with one and two coats of a coating product. EIS should be used to measure impedance during the tests to determine the effect of two coats.

A clear effect of T_g-region on revisability and temperature dependence of impedance was observed for one coating. The test procedure that was used in this work can be applied in further work on other coating products to gain knowledge about the effect of T_g-region on impedance.

References

[1] J. Henry Leidheiser, *Corrosion Control by Organic Coatings*. Houston: NACE, 1981.

[2] H. Bi and J. Sykes, "An investigation of cathodic oxygen reduction beneath an intact," *Progress in Organic Coatings,* pp. 83-87, 2015.

[3] H. Leidheiser and W. Wang, "Some Substrate and Environmental Influences on the Cathodic Delamination of Organic Coatings," *Journal of Coatings Technology,* vol. 53, no. 672, pp. 77-84, 1981.

[4] O. Ø. Knudsen and A. Forsgren, *Corrosion control through organic coatings*. Trondheim: Taylor & Francis Group, 2017.

[5] O. Ø. Knudsen and J. I. Skar, "Cathodic Disbonding of Epoxy Coatings- Effects of Test Parameters," *NACE- Intenrational Corrosion Conference Series,* 2008.

[6] P. A. Sørensen, C. E. Weinell, K. Dam-Johansen, and S. Kiil, "Reduction of cathodic delamination rates of anticorrosive coatings using free radical scavengers," *Journal of Coatings Technology and Research,* vol. 7, pp. 773-786, 2010.

[7] G. P. Bierwagen, L. He, J. Li, L. Ellingson, and D. E. Tallman, "Studies of a new accelerated evaluation method for coating corrosion resistance- thermal cycling testing," *Progress in Organic Coatings* vol. 39, pp. 67-78, 2000.

[8] J. F. Watts, "Mechanistic Aspects of the Cathodic Delamination of Organic Coatings," *The Journal of Adhesion,* vol. 31, no. 1, pp. 73-85, 1989.

[9] T. Bos, "durability, Prediction of coating- Early detection using electrochemical methods," Gildeprint drukkerijen B.V., Enschede, The Netherlands, 2008.

[10] K. B. Tator, *Coating Deterioration- ASM Handbook, Volume 5B, Protective Organic Coatings*. ASM International, 2015.

[11] M. Stratmann, R. Feser, and A. Leng, "Corrosion Protection by Organic Films," *Electrochemica Acta,* vol. 39, no. 8-9, pp. 1005-1358, 1994.

[12] J. Henry Leidheiser, "Electrochemical Methods for Appraising Corrosion Protective Coatings," *Journal of Organic Coatings Technology,* vol. 63, no. 802, pp. 21-31, 1991.

[13] J. Parks and J. Henry Leidheiser, "Ionic Migration through Organic Coatings and Its Consequences to Corrosion," *Ind. Eng. Chem. Prod. Res. Dev. ,* vol. 25, no. 1, pp. 1-6, 1986.

[14] G. Bierwagen, J. Li, N. Davis, and D. Tallman, "Thickness Dependence of Electrochemical Properties of Organic Coatings," in *Proceedings of the Fifth Nürnberg Congress, Vol. 1*, Nürnberg, 1999.

[15] R. C. Bacon, J. J. Smith, and F. M. Rugg, "Electrolytic Resistance in Evaluating Protective Merit of Coatings on Metals," Bakelite Corporation, Bloomfield, New Jersey, 1948.

[16] G. Bierwagen, D. Tallman, J. Li, L. He, and C. Jeffcoate, "EIS studies of coated metals in accelerated exposure," *Progress in Organic Coatings* vol. 46, pp. 148-157, 2003.

[17] O. Knudsen, C. Hagen, A. Skilbred, A. Løken, D. Höche, and B. Daneshian, "Correlation between standard laboratory coating tests and field testing," in *The European Corrosion Congress*, 2021.

[18] A. L. H. S. M. Stratmann, "The delamination of polymeric coatings from steel. Part 1: Calibration of the Kelvinprobe andbasic delamination mechanism," *Corrosion Science,* vol. 41, pp. 547-578, 1999.

[19] A. Rudin and P. Choi, *The Elements of Polymer Science & Engineering (Third Edition)*. Academic Press, 2013.

[20] S. Shreepathi, "Physicochemical parameters influencing the testing of cathodic delamination resistance of high build pigmented epoxy coating," *Progress in Organic Coatings,* vol. 90, pp. 438-447, 2016.
[21] J. Mijovic and K.-F. Lin, "The Effect of Hygrothermal Fatigue on Physical/ Mechanical Properties and Morphology of Neat Epoxy Resin and Graphite/Epoxy Composite," *Journal of Applied Polymer Science,* vol. 30, pp. 2527- 2549, 1985.
[22] M. Wang, X. Xub, J. Ji, Y. Yang, J. Shen, and M. Ye, "The hygrothermal aging process and mechanism of the novolac epoxy resin," *Composites,* vol. 107, pp. 1-8, 2016.
[23] G. Z. Xiao and M. E. R. Shanahan, "Swelling of DGEBA/DDA epoxy resin during hygrothermal ageing " *Polymer* vol. 39, no. 14, pp. 3253- 3260, 1998.
[24] S. González, M. A. Gil, J. O. Hernández, V. Fox, and R. M. Souto, "Resistance to corrosion of galvanized steel covered with an epoxy-polyamide primer coating," *Progress in Organic Coatings,* vol. 41, pp. 167-170, 2001.
[25] O. Ø. Knudsen and U. Steinsmo, "Effect of Barrier Pigments on Cathodic Disbonding Part 2: Mechanism of the Effect of Aluminium Pigments," *Journal of Corrosion Science and Engineering,* vol. 2, 1999.
[26] X. H. Jin, K. C. Tsay, A. Elbasir, and J. D. Scantlebury, "The Adhesion and Disbonding of Chlorinated Rubber on Mild Steel," in *Proceedings of the Symposium On Corrosion Protection by Organic Coatings*, 1989.
[27] H. L. Jr., W. Wang, and L. Igetoft, "The Mechanism for the Cathodic Delamination of Organic Coatings from a Metal Surface," *Progress in Organic Coatings,* vol. 11, pp. 19-40, 1983.
[28] A. M. Lowe, "Estimation of Electrochemical Noise Impedance and Corrosion Rates from Electrochemical Noise Measurement," Curtin University of Technology, Curtin, 2002.
[29] D. Collins. (2020, September 15) What's the difference between resistance, reactance, and impedance? *Motion Control Tips*. URL: https://www.motioncontroltips.com/whats-the-difference-between-resistance-reactance-and-impedance/ Accessed: 25.08.2021.
[30] G. Instruments, *Basics of Electrochemical Impedance Spectroscopy*. Accessed: 30.08.2021: Gamry Instruments, URL: https://www.gamry.com/application-notes/EIS/basics-of-electrochemical-impedance-spectroscopy/.
[31] A. Amirudin and D. Thierry, "Application of electrochemical impedance spectroscopy to study the degradation of polymer-coated metals " *Progress in Organic Coatings,* vol. 26, pp. 1-28, 1995.
[32] F. Mansfeld, "Use of electrochemical impedance spectroscopy for the study of corrosion protection by polymer coatings," *Journal of Applied Electrochemistry,* vol. 25, pp. 187-202, 1995.
[33] "Selecting a Reference Electrode," URL: http://www.consultrsr.net/resources/ref/select.htm, Accessed: 13.10.2021, 2014.
[34] *Risks of Using Additional Cabling* Url: https://www.gamry.com/application-notes/instrumentation/additional-cabling/: gamry.com, Accessed: 04.10.2021.
[35] J. C. M. R. J. B. H. A. Foster, "On the Nature of Epoxy Resin Post-Curing," *Polymers,* vol. 12, 2020.
[36] X. P. F. L. C. H. P. Fang, "Effect of Curing Agents on the Photodegradation of Epoxy Coatings investigated by Electrochemical Impedance Spectroscopy," *Int. J. Electrochem. Sci.,* vol. 13, pp. 8944 – 8952, 2018.
[37] M. R. D. C. B. C. F. I. B. d. B. J. B. d. C. I. N. B. H. R. M. Costa, "Evaluation of adhesion of epoxy resin sealant to improve the corrosion resistance of thermal sprayed coatings," *Applied Adhesion Science* vol. 8, 2020.

Appendix

Appendix A: Complete Film Thickness Description of All Coating Samples

Parallel 1		
Coating	NDFT	DFT
A	1 X 180 µm	168 µm
B	1 X 180 µm	188 µm
C	2 X 175 µm	385 µm
D	2 X 175 µm	370 µm
E	1 X 250 µm	266 µm
F	1 X 250 µm	286 µm

Parallel 2		
Coating	NDFT	DFT
A	1 X 180 µm	167 µm
B	1 X 180 µm	216 µm
C	2 X 175 µm	414 µm
D	2 X 175 µm	394 µm
E	1 X 250 µm	272 µm
F	1 X 250 µm	305 µm

Parallel 3		
Coating	NDFT	DFT
A	1 X 180 µm	230 µm
B	1 X 180 µm	200 µm
C	2 X 175 µm	417 µm
D	2 X 175 µm	358 µm
E	1 X 250 µm	267 µm
F	1 X 250 µm	310 µm

Parallel 4		
Coating	NDFT	DFT
A	1 X 180 µm	203 µm
B	1 X 180 µm	203 µm
C	2 X 175 µm	406 µm
D	2 X 175 µm	385 µm

Parallel 5		
Coating	NDFT	DFT
A	1 X 180 µm	206 µm
B	1 X 180 µm	212 µm

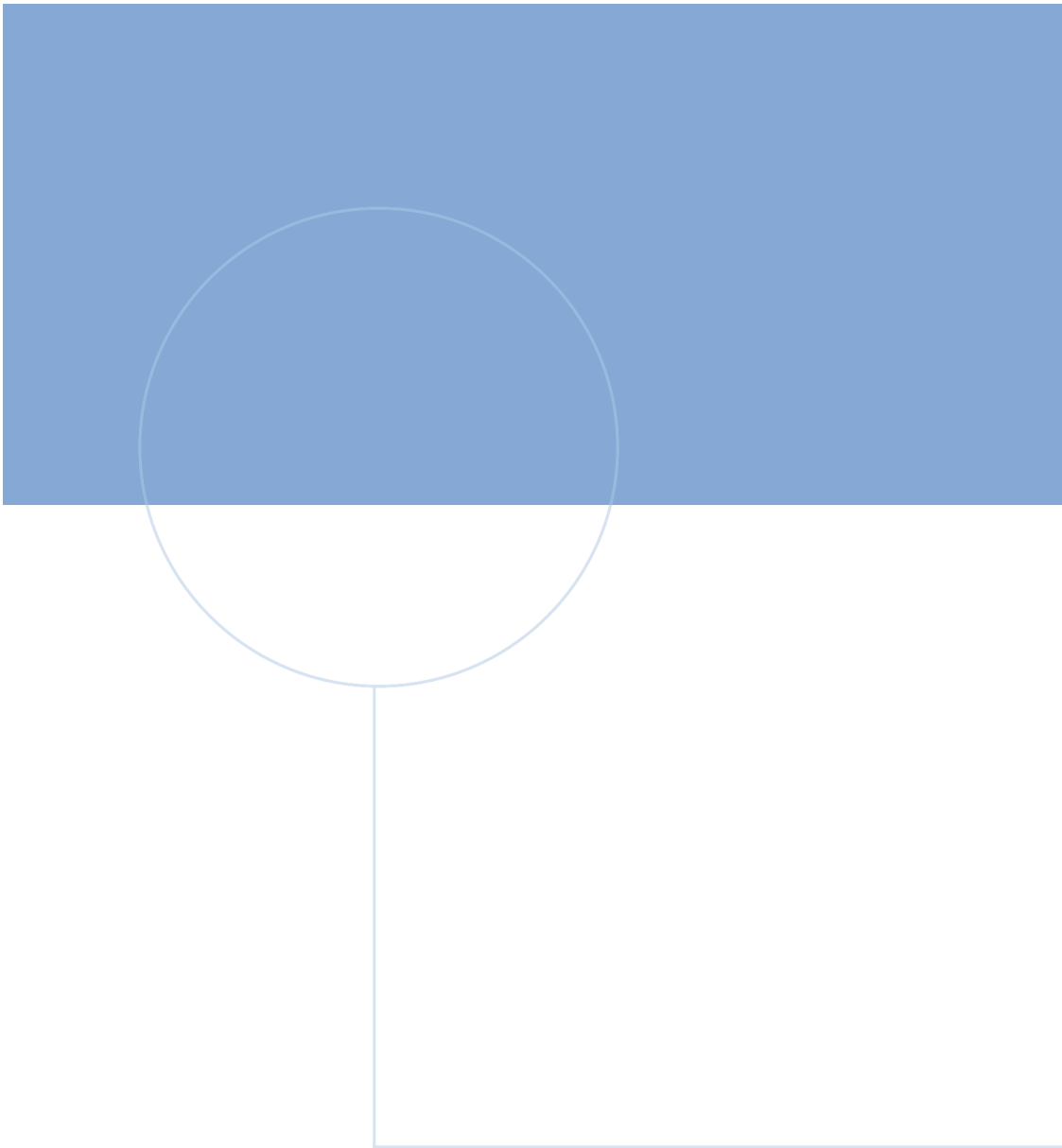

NTNU

Norwegian University of
Science and Technology